Mathematical Biosciences 304 (2018) 9–24

Contents lists available at ScienceDirect

Mathematical Biosciences

journal homepage: www.elsevier.com/locate/mbs

Practical identifiability and uncertainty quantification of a pulsatile cardiovascular model

Andrew D. Marquis[a,b], Andrea Arnold[b,c], Caron Dean-Bernhoft[d], Brian E. Carlson[a], Mette S. Olufsen[*,b]

[a] University of Michigan, Ann Arbor, MI, USA
[b] NC State University, Raleigh, NC, USA
[c] Worcester Polytechnic Institute, Worcester, MA, USA
[d] Medical College of Wisconsin, Milwaukee, WI, USA

ARTICLE INFO

Keywords:
Cardiovascular dynamics
Modeling
Parameter estimation
Uncertainty quantification
Patient-specific modeling

ABSTRACT

Mathematical models are essential tools to study how the cardiovascular system maintains homeostasis. The utility of such models is limited by the accuracy of their predictions, which can be determined by uncertainty quantification (UQ). A challenge associated with the use of UQ is that many published methods assume that the underlying model is identifiable (e.g. that a one-to-one mapping exists from the parameter space to the model output). In this study we present a novel workflow to calibrate a lumped-parameter model to left ventricular pressure and volume time series data. Key steps include using (1) literature and available data to determine nominal parameter values; (2) sensitivity analysis and subset selection to determine a set of identifiable parameters; (3) optimization to find a point estimate for identifiable parameters; and (4) frequentist and Bayesian UQ calculations to assess the predictive capability of the model. Our results show that it is possible to determine 5 identifiable model parameters that can be estimated to our experimental data from three rats, and that computed UQ intervals capture the measurement and model error.

1. Introduction

Precision medicine is a growing model of healthcare that proposes to customize of care, medical decisions, practices, and products to each individual patient. This approach is important, as pathologies such as cancer, autoimmune disorders, and cardiovascular diseases are unique to a given individual making it challenging to develop diagnostic and treatment protocols. One approach, to studying patient-specific complexities, is to use mathematical modeling to estimate function and predict features that are difficult to measure, thus providing a more comprehensive set of information to distinguish between individual patients.

A rich history of cardiovascular modeling exists in the literature, typically presented either from a fluid dynamics perspective (resulting in systems of PDEs) [1–3] to study local flow properties, or from a compartment perspective (resulting in systems ODEs) to study systems level dynamics [4,5]. The model type used depends on the questions investigated. Fluid dynamics models (1D-3D) are excellent for examining flow properties, e.g. how local flow is impacted by geometric structure, such as flow past a stent, flow changes following bypass surgery, flows in aneurysms, valves function, or flow and wave propagation changes in hypertension or diabetes [6–11]. However, due to computational complexity, 1D-3D models are typically not used in studies aiming to understand how the CV system interacts with other systems, e.g. autonomic control by neuro-humoral mechanisms, the immune system, or physiologically-based pharmacokinetics [12–14]. The main obstacle is that models used in this setting often need to be solved over long time-scales. For these types of applications compartment ODE models are more appropriate. One disadvantage to ODE models is that they are difficult to parameterize and fit to data. To illustrate the steps associated with this process we have chosen to analyze a simple 5-compartment (0D) model inspired by models used to predict changes during head-up tilt [15]. In ODE models, compartments represent groups of vessels (e.g. large or small arteries or veins, capillaries, or vessels supplying specific tissues or organs) coupled to a heart compartment that act as a pump to drive the system. Some models include both pulmonary and systemic circulations [16], while others analyze one of the two systems [17]. ODE models of this type can be used to extract vascular properties such as vascular resistance, cardiac contractility, or compliance by fitting models to pressure and flow data

* Corresponding author.
E-mail address: msolufse@ncsu.edu (M.S. Olufsen).

https://doi.org/10.1016/j.mbs.2018.07.001
Received 11 December 2017; Received in revised form 1 May 2018; Accepted 2 July 2018
Available online 11 July 2018
0025-5564/

from noninvasive imaging studies [15,18,19] and/or from invasive catheterization [20–22] studies.

One of the biggest challenges in calibrating compartment models to data is obtaining accurate parameter estimates. Even in its basic form, where the model is formulated using systems of linear differential equations, forced by a contracting heart, it is typically not possible to uniquely estimate all model parameters. To overcome this, we use sensitivity analysis and subset selection for *a-priori* study of the model structure followed by parameter estimation and uncertainty quantification. In general, parameters that are unidentifiable as a result of model structure are referred to as *structurally unidentifiable* [23], whereas parameters that are unidentifiable as a result of practical restrictions, such as availability and quality of data, are referred to as *practically unidentifiable* [24]. Theoretically, structural identifiability is a prerequisite for practical identifiability. However, in practice it can be difficult to establish the former, since analysis is restricted to models for which it is possible to define a unique input-output relation [23].

Only a few studies have addressed structural identifiability in cardiovascular models. Kirk et al. [25], studying Windkessel models, showed that three of four parameters are identifiable, and Pironet et al. [26] demonstrated that every parameter in a linear six-compartment model including a left and right heart, systemic and pulmonary arteries and veins are structurally identifiable if outputs contain both pressure (in all arteries and veins) and left/right ventricular stroke volume, while models relying on either pressure or volume alone are structurally unidentifiable. Other studies have employed sensitivity and practical, opposed to structural, identifiability analysis to predict arterial blood pressure and cardiac output [15,19,27,28]. Several recent studies have addressed uncertainty quantification, mostly for analysis of 1D fluid dynamics models. To our knowledge, these methodologies have not previously been applied to analysis of compartment models. The study by Eck et al. [29] developed a guide to uncertainty quantification in cardiovascular models presenting a number of methodologies. Several studies have predicted uncertainties in specific one-dimensional fluid mechanics models [30–35]. Of these, three studies accounted for uncertainty using Kalman filtering [30–32], two used polynomial chaos expansion, and one [35] used an MCMC approach based on the Delayed Rejection Adaptation Metropolis (DRAM) algorithm [36]. To our knowledge, none of these studies combined these techniques into an organized workflow for the determination of model parameters in compartmental CV models given a specific data set.

In this study, we present a general multi-stage workflow applied to analysis of a five compartment model for the systemic circulation with left ventricular volume and blood pressure data from three Sprague Dawley rats. The key steps in our workflow include: (1) the use of literature and available data to compute nominal parameter values specific to each rat; (2) sensitivity analysis and subset selection to determine a set of identifiable parameters; (3) optimization to compute point estimates for the identifiable parameters; and (4) statistical techniques to quantify uncertainty of the model output.

2. Methods

2.1. Experimental data

Data analyzed here are extracted from experiments performed on 3 Sprague-Dawley (SD) rats (2 male, 1 female). The average weight of these animals was 358.0 ± 19.6 g. The rats were anesthetized with sodium pentobarbital (50 mg/kg, ip), and catheters were placed in a femoral vein and artery for administration of anesthetics and monitoring of systemic blood pressure, respectively. A pressure-volume conductance catheter (Millar SPR-869, 2F tip with four electrodes and 6 mm spacing) was inserted through the right carotid artery into the left ventricle. For each rat basic physiological measures (sex, weight, heart rate, average stroke volume and cardiac output, Table 1) were recorded along with continuous measurements of left ventricular volume and pressure. For this study, approximately 20-second time-series data, measured at rest, were selected for model identification and the final 0.5 s of each data set was used to calibrate the model, shown in Fig. 1.

Table 1
Rat average data.

Rat	Sex	Weight (g)	Heart rate (beats/min)	Stroke volume (μl)	Cardiac output (ml/min)
Rat 1	Male	339	240 ± 3	308 ± 1	74 ± 0.2
Rat 2	Male	350	240 ± 3	216 ± 1	52 ± 0.2
Rat 3	Female	342	420 ± 3	143 ± 1	60 ± 0.2

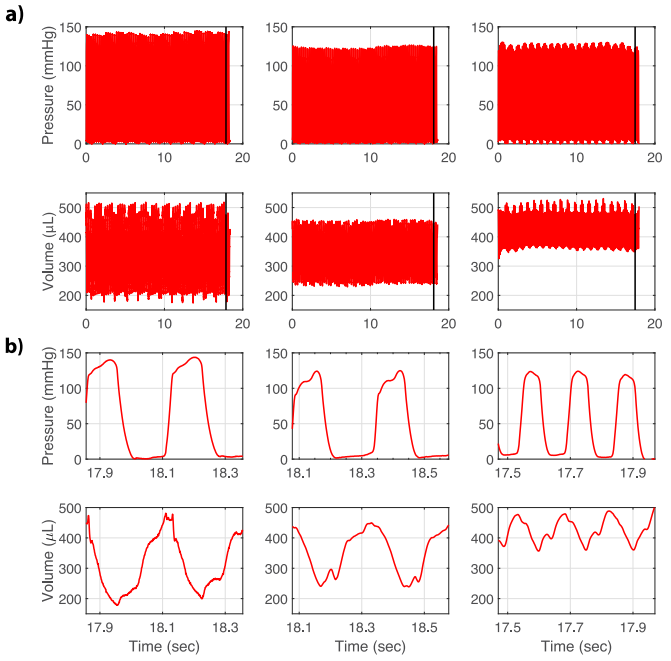

Fig. 1. Left ventricle pressure and volume data from three rats. Each column corresponds to a different rat. **(a)** shows the 20-second raw time-series data and **(b)** shows a zoomed-in view of the final 0.5 s used to calibrate the model output (marked by vertical black lines on the top two rows.).

Volume-conductance calibration

One of the most common methods for translating conductance measurements to volume is using Baan's equation

$$V(t) = \frac{L^2}{\alpha\sigma}[G(t) - G^p],$$

where $V(t)$ is the left ventricular volume, L is the spacing between electrodes on the catheter, σ is the specific conductivity of the blood, $G(t)$ is the measured total conductance (measured as a voltage directly proportional to the conductance), G^p is the parallel conductance through the myocardium, and α is a stroke volume scaling factor determined from cuvette calibration, obtained by infusing a known hypertonic saline bolus before the experiment and extracting known volumes after the experiment. This allows subtraction of parallel conductance through the myocardium from the total measured conductance.

In this study, the baseline left ventricular pressure and volume time-course analyzed is extracted from a longer experimental time-course involving sequential blood withdrawals. This experimental manipulation (blood withdrawal) violates the assumption of constant σ, G^p (and possibly α) in Baan's equation. It has previously been found that the volume-voltage relationships determined using cuvette calibration measures is highly sensitive to changes in hematocrit and hence conductivity of blood [21,37]. Furthermore, sufficient loss of blood

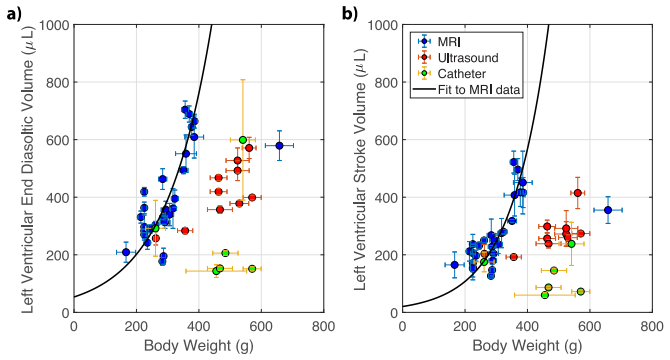

Fig. 2. Left ventricular EDV (**a**) and SV (**b**) as a function of animal weight and exponential fits (using (1) to literature data from catheter [39–58] and MRI-based measurement modalities [40,41,43,45–48,50,53–57]. Error bars denote the standard deviation from each study.

volume could compromise hemodynamics such as a reduced stroke volume.

Therefore, to obtain volumes within a standard physiological range, the cuvette measures were scaled against literature estimates pooling end diastolic and stroke volume data from 20 previously published studies using conduction catheters, ultrasound, and magnetic resonance imaging (MRI) of the left ventricle in SD, Wistar-Kyoto, and Lewis rat strains (from 191 animals total). These data are shown as a function of animal body weight in Fig. 2. Since MRI based volume measurement techniques have been adopted as the gold-standard for ventricular volume studies [38], one can observe that measurements from non-MRI methods tend to under estimate both the end diastolic and stroke volume. To obtain realistic volumes, we fit 13 MRI-based end diastolic and stroke volume data sets to body weight using exponential functions

$$\begin{aligned} \text{EDV} &= a\exp\left(b\left(\frac{\text{BW}}{250\text{g}}-1\right)\right) \quad \text{and} \\ \text{SV} &= c\exp\left(d\left(\frac{\text{BW}}{250\text{g}}-1\right)\right), \end{aligned} \tag{1}$$

where BW is the body weight, EDV is the end diastolic volume, SV is the stroke volume, and $\{a, b, c, d\}$ are estimated parameters. Predicted values of EDV and SV from (1) are calculated for each animal in our study. The predicted EDV is used to convert the peak conductance for each cardiac cycle to the maximum volume and the predicted SV is used to scale the amplitude of the conductance signal. A more detailed calibration procedure is provided in the Appendix.

2.2. Model

As noted earlier this study focus on analysis of compartment models used in studies designed to investigate dynamics over longer timescales (min-hours) [12–14]. The objective here is to design a workflow illustrating how to calibrate and validate this model type. To understand how changes in input (venous properties) have on the output (arterial properties) we chose to build a closed loop systemic model, omitting the pulmonary circulation. Since the left heart pumps into the systemic circulation we chose to include this as part of the feedback. To predict "waveforms" with some dissipation through the system we included two arterial and venous compartments. The resulting model is similar to previous models [15,19] using a five-compartment model to predict hemodynamics pressure, flow, and volume in the left ventricle, the large and small arteries and veins; see Fig. 3. The basic assumptions for this model type, is that hemodynamics can be described using an electrical circuit analogy, in which blood flow (q) is analogous to current, pressure (p) to voltage, volume (V) to charge, vessel resistance (R) to electric resistance, and vessel elastance (E) to the reciprocal of

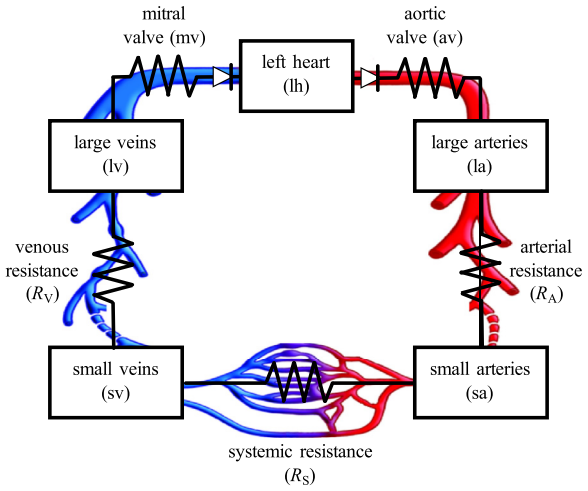

Fig. 3. Systemic circulation represented using five compartments, including the left heart (lh) (e.g., the left ventricle), the large (la) and small (sa) systemic arteries, and the large (lv) and small (sv) systemic veins. The model is analogous to an RC circuit with capacitors denoting vessel elastance and resistors separating each compartment. Pumping of the heart is ensured by a time-varying elastance function (5).

capacitance. For each compartment, dynamics are predicted from three equations relating pressure, flow and volume. The flow in and out of each compartment is proportional to pressure via Ohm's law

$$q = \frac{p_{\text{in}} - p_{\text{out}}}{R}; \tag{2}$$

the pressure and volume in each compartment is related to elastance via

$$p - p_{\text{ext}} = E(V - V_{\text{un}}) = EV_{\text{str}}, \tag{3}$$

where p_{ext} is the external tissue pressure, V_{un} is the unstressed blood volume (both assumed constant), and V_{str} is the stressed blood volume; and conservation of volume gives

$$\frac{dV}{dt} = \frac{dV_{\text{str}}}{dt} = q_{\text{in}} - q_{\text{out}}. \tag{4}$$

For the circuit shown in Fig. 3, we derive a system of five differential equations for the stressed volume of the form (4), detailed in the Appendix. The beating of the heart (Fig. 4) is modeled by a periodic time-varying elastance function [27] defined over one cardiac cycle of length T as

$$E_{\text{lh}}(t) = \begin{cases} E_{\text{m}} + \dfrac{E_{\text{M}} - E_{\text{m}}}{2}(1 - \cos(\pi t/T_{\text{S}})) & 0 < t < T_{\text{S}} \\ E_{\text{m}} + \dfrac{E_{\text{M}} - E_{\text{m}}}{2}\cos(\pi(t - T_{\text{S}})/(T_{\text{R}} - T_{\text{S}})) & T_{\text{S}} < t < T_{\text{R}} \\ E_{\text{m}} & T_{\text{R}} < t < T, \end{cases} \tag{5}$$

where E_{m} and E_{M} denote the minimum and maximum elastance, respectively, of the left ventricle. T_{S} denotes time for end systole and T_{R} the time at which the heart has relaxed to its diastolic value. We model the two heart valves using its electrical equivalent, a diode, i.e.

$$q_{\text{valve}} = \begin{cases} \dfrac{p_{\text{in}} - p_{\text{out}}}{R_{\text{valve}}} & \text{if } p_{\text{in}} > p_{\text{out}} \text{ (e.g., if valve is open)} \\ 0 & \text{otherwise (e.g., if valve is closed),} \end{cases} \tag{6}$$

where valve = av or mv, representing the aortic (av) and mitral (mv) valves, respectively.

In summary, the model takes the form

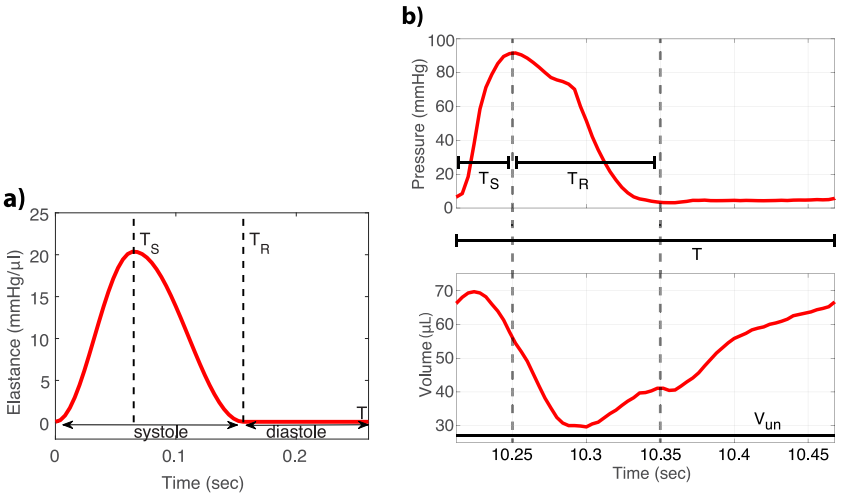

Fig. 4. The time-varying elastance is modeled using a smooth piecewise trigonometric function defined over the length of one cardiac cycle T (given by Eq. (5)). Maximum elastance E_M is achieved at $t = T_S$ (at the end of systole) and the end contraction is marked by $t = T_R$. Plots of the elastance function (**a**) and representative pressure and volume data (**b**) are shown to illustrate how the timing parameters T_S and T_R are estimated (see Section 2.3).

$$\begin{aligned}\frac{dx}{dt} &= f(x, t; \theta), x(0) = x_0\\ x &= \{V_{lh}, V_{la}, V_{sa}, V_{sv}, V_{lv}\}\\ \theta &= \{R_A, R_S, R_V, E_{la}, E_{sa}, E_{sv}, E_{lv}, T_S, T_R, E_m, E_M\}\\ y &= \{V_{lh}, P_{lh}\},\end{aligned}$$

where x denotes the model states, θ the model parameters, and y the model output.

2.3. Nominal parameters and initial values

Nominal parameters and initial conditions for the ODEs can be obtained from analysis of data and known physiological features extracted from literature. In this study, parameters include resistance, elastance, and timing of the cardiac cycle, which are determined as a function of resting blood volumes, pressures, cardiac output, and heart rate. In the following sections we discuss how to calculate *a priori* values for all model parameters, listed in Table 2.

2.3.1. Blood volume

Total blood volume for healthy adult Wistar rats is 57μl/g body weight [59] (listed in Table 1). Measurements analyzed in this study are from 2 male and 1 female healthy Sprague Dawley rats (Charles River Laboratories, USA). Following suggestions by Young [60] and Gelman [61], the total volume for the purpose of nominal value estimation is distributed with 2.5% in the large arteries, 7.5% in the large veins, 20% in the small arteries and 70% in the small veins to 70%, i.e. for each compartment, the volume is given by

$$V_i = d_i V_{\text{total}}, \tag{7}$$

where V_{total} is the total blood volume, V_i refers to the i'th compartment volume, and d_i denotes the percentage of the total blood volume to compartment i.

As noted above, the model is formulated in stressed volume, which is a small percentage of the total blood volume. Literature estimates for the total stressed volume vary significantly, from about 10% to 40% [59–63]. We found no resources describing distribution of stressed and unstressed volume across organs or between arteries and veins in rats, therefore we used the same stressed volume fraction (30%) in all

Table 2
Quantities used to determine nominal parameter estimates.

Quantity	Equation	Reference	Quantity	Equation	Reference
V_{la}	$0.025\,V_{\text{total}}$	[60,61]	$p_{la,M}$	$0.99\max(p_{lh,d})$	data
			$\bar{p}_{la}$	$p_{la,dia} + 1/3\,p_{la,pulse}$	[64]
V_{sa}	$0.2\,V_{\text{total}}$	[60,61]	$p_{sa,M}$	$0.99\,p_{la,M}$	data
			$\bar{p}_{sa}$	$p_{sa,dia} + 1/3\,p_{sa,pulse}$	[64]
V_{lv}	$0.075\,V_{\text{total}}$	[60,61]	$\bar{p}_{lv}$	$1.1\min(p_{lh,d})$	data
V_{sv}	$0.7\,V_{\text{total}}$	[60,61]	$\bar{p}_{sv}$	$1.1\,\bar{p}_{lv}$	data
R_{av}	$\frac{\max(p_{lh,d}) - p_{la,M}}{CO}$	(10)	E_{la}	$\frac{p_{la,M}}{V_{la} - V_{la,un}}$	(11)
R_{mv}	$\frac{\bar{p}_{lv} - \min(p_{lh,d})}{CO}$	(10)	E_{sa}	$\frac{p_{sa,M}}{V_{sa} - V_{sa,un}}$	(11)
R_A	$\frac{\bar{p}_{la} - \bar{p}_{sa}}{CO}$	(9)	E_{lv}	$\frac{\bar{p}_{lv}}{V_{sv} - V_{sv,un}}$	(11)
R_S	$\frac{\bar{p}_{sa} - \bar{p}_{sv}}{CO}$	(9)	E_{sv}	$\frac{\bar{p}_{sv}}{V_{sv} - V_{sv,un}}$	(11)
R_V	$\frac{\bar{p}_{sv} - \bar{p}_{lv}}{CO}$	(9)			
T_S	$t_{\max(V_{lh,d})}$		E_M	$\frac{\bar{p}_{lv}}{\max(V_{lh,d}) - V_{lh,un}}$	(12)
T_R	$t_{\min(p_{lh,d})}$		E_m	$\frac{p_{la,dia}}{\min(V_{lh,d}) - V_{lh,un}}$	(12)

compartments, i.e.

$$V_{i,\mathrm{str}} = 0.3\,V_i, \quad \text{for all } i, \tag{8}$$

where i denotes "left heart" (lh), "large arteries" (la), "small arteries" (sa), "small veins" (sv), or "large veins" (lv).

2.3.2. Pressure

Measurements of left ventricular pressure is used to approximate pressures in all vascular compartments. Starting at the large arteries, the aortic valve open when the pressure in the left ventricle exceeds the aortic pressure. The maximum pressure in the systemic arteries follow the one in the left ventricle. Assuming a constant pressure drop from left ventricle through the small arteries we let

$$p_{\mathrm{la,M}} = 0.99\max(p_{\mathrm{lh,d}}), \quad p_{\mathrm{sa,M}} = 0.99p_{\mathrm{la,M}},$$

where $p_{\mathrm{lh,d}}$ denotes the left ventricular pressure data, $p_{\mathrm{la,M}}$ denotes maximum larger artery pressure, and $p_{\mathrm{sa,M}}$ denotes maximum small artery pressure. Without pressure measurements in the systemic arteries, more assumptions are needed to approximate the mean arterial pressure. Assuming a pulse pressure of $p_{\mathrm{a,pulse}} = 30$ mmHg, large and small artery diastolic pressure can be estimated as $p_{\mathrm{la,dia}} = p_{\mathrm{la,M}} - p_{\mathrm{a,pulse}}$, and $p_{\mathrm{sa,dia}} = p_{\mathrm{sa,M}} - p_{\mathrm{a,pulse}}$ from which we can estimate mean arterial blood pressure as

$$\overline{p}_{\mathrm{la}} = p_{\mathrm{la,dia}} + 1/3\,p_{\mathrm{a,pulse}}, \quad \overline{p}_{\mathrm{sa}} = p_{\mathrm{sa,dia}} + 1/3\,p_{\mathrm{a,pulse}}$$

using the common clinical approximation [64].

This model does not represent the right ventricle or pulmonary vasculature so the pressure in the systemic veins becomes the filling pressure for the left ventricle. Thus similar to the arterial side, we assume a 10% pressure drop between large and small veins, so we let

$$\overline{p}_{\mathrm{lv}} = 1.1\min(p_{\mathrm{lh,d}}), \quad \overline{p}_{\mathrm{sv}} = 1.1\overline{p}_{\mathrm{lv}},$$

2.3.3. Cardiac output

For each rat, the average stroke volume (Table 1) is extracted from measurements of maximum and minimum left ventricular volume. Cardiac output can subsequently be calculated as the product of stroke volume and heart rate (i.e. CO = HR V_{stroke}).

2.3.4. Vascular resistance

Using the baseline cardiac output and pressure, the vascular resistances can be computed from Ohm's law (2). For example, arterial resistance is predicted as

$$R_{\mathrm{A}} = \frac{\overline{p}_{\mathrm{la}} - \overline{p}_{\mathrm{sa}}}{\mathrm{CO}}. \tag{9}$$

Instead of using the mean pressures to calculate valve resistance we consider the maximum and minimum pressure to estimate the resistance across the aortic and mitral which can be expressed as

$$R_{\mathrm{av}} = \frac{\max(p_{\mathrm{lh,d}}) - p_{\mathrm{la,M}}}{\mathrm{CO}} \quad \text{and} \quad R_{\mathrm{mv}} = \frac{\overline{p}_{\mathrm{lv}} - \min(p_{\mathrm{lh,d}})}{\mathrm{CO}}, \tag{10}$$

where R_{av} is the aortic valve resistance and R_{mv} is the mitral valve resistance. Since the venous pressure do not vary significantly, the average pressure of the large veins is used to predict R_{mv}.

2.3.5. Vascular compliance

Each vascular compartment is associated with an elastance (constant). Assuming that the tissue pressure is negligible (e.g. $p_{\mathrm{ext}} = 0$), elastance can be estimated as

$$E_{\mathrm{la}} = \frac{p_{\mathrm{la,M}}}{V_{\mathrm{la}} - V_{\mathrm{la,un}}}, \tag{11}$$

following the pressure-volume relation (3), set up for the large arteries as a representative example.

2.3.6. Heart parameters

The elastance function (5) has four parameters, including timing parameters denoting the length of the cardiac contraction (T_{S}) and relaxation (T_{R}), as well as the minimum (E_{m}) and maximum (E_{M}) elastance. Rat unstressed ventricular volume has been estimated at 37μl [65]. For each rat, the timing parameters T_{S} and T_{R} can be extracted from data, as shown in Fig. 4. T_{S} denotes the time at which the left ventricular volume reaches it maximum (at $\max(p_{\mathrm{lh,d}})$), and T_{R} is the time at which p_{lh} reaches its baseline after contraction. The minimum elastance E_{m} is associated with end-diastole, where the left ventricular pressure is minimal and ventricular volume is maximal, and the maximum elastance E_{M} is associate with systole, where the ventricular pressure is maximal and ventricular volume is minimal. These considerations let us set

$$E_{\mathrm{m}} = \frac{\min(p_{\mathrm{lh,d}})}{\max(V_{\mathrm{lh,d}}) - V_{\mathrm{lh,un}}} \quad \text{and}$$
$$E_{\mathrm{M}} = \frac{\max(p_{\mathrm{lh,d}})}{\min(V_{\mathrm{lh,d}}) - V_{\mathrm{lh,un}}}. \tag{12}$$

2.3.7. Initial conditions

Assuming that the model simulation begins at the end of systolic contraction (beginning of diastolic filling), we set the initial value of the volume in each compartment to their stressed volume ($V_{i,\mathrm{s}}$). This implies that

$$V_{0,i} = V_{i,\mathrm{s}} = 0.3V_i \tag{13}$$

where $V_{0,i}$ is the initial volume of the i'th compartment.

3. Model analysis

The model described in Section 2.2 is linear with respect to the states but nonlinear with respect to the parameters. This gives rise to multiple parameter interactions that inevitably complicate the parameter estimation process. While a model with many nonlinear parameter interactions can be structurally identifiable, unidentifiable parameter relationships often result in an ill-conditioned optimization problem [66].

In this section, we outline a systematic workflow for parameter estimation, comprising identification of

1. *Nominal parameters* from literature and available data followed by a baseline simulation to ensure an appropriate model response. For the model analyzed here this step requires two parts: (i) using data to compute subject specific nominal parameter values, (ii) determine a shift in data to ensure that model predictions and data are in phase.
2. *Local sensitivities* used to study how the parameters influence the model output.
3. *Structured correlations* used to determine a subset of parameters with minimal parameter interactions.
4. *Parameter estimates* obtained using the Levenberg–Marquardt optimization method, estimating the subset of identifiable parameters minimizing the least squares error between the model output and available data.
5. *Frequentist prediction and confidence intervals* used to quantify uncertainty in the model solutions.
6. *Parameter distributions and credible intervals* obtained using the DRAM (Delayed Rejection Adaptive Metropolis) algorithm.

While the analysis is devised for a relatively simple cardiovascular model with a specific set of output data (left ventricular pressure and volume), the approach introduced here is applicable to any predictive model fitted to time-varying data. Obtaining the nominal parameter of step one is model specific however, steps 2–6 are more generic and the

approach presented here can be more generally applied.

3.1. Local sensitivity analysis

Sensitivity analysis quantifies how the model output changes in response to changes in parameter values [27]. In this study we use derivative-based sensitivities to quantify the local influence of the model output on each parameter. Similar to the study by Pope et al. [19], we computed sensitivities from partial derivatives of the model output residual with respect to each model parameter, i.e. we define the sensitivity matrix S as

$$\mathsf{S}_{i,j} = \frac{\partial r(t_i, \theta)}{\partial \theta_j}, \tag{14}$$

where θ_j is the j'th parameter and t_i is the i'th time step. When estimating parameters in a log-transformed space (14) can be expressed as

$$\frac{\partial r(t_i, \theta)}{\partial \ln(\theta_j)} = \theta_j \frac{\partial r(t_i, \theta)}{\partial \theta_j}.$$

The matrix S can be calculated analytically for simple models; however, numerical approximation of S is more practical for complex models. Here we employ finite differences to approximate S by

$$\mathsf{S}_{i,j} = \frac{r(t_i, \theta_j + he_i) - r(t, \theta_j)}{h},$$

where h is chosen to reflect the precision of the model output and e_i is the unit vector in the i'th component direction. If the error in the model evaluation (ODE solver error tolerance) is on the order of ε, the step should be $h = \sqrt{\varepsilon}$ to get an error of the same magnitude in the sensitivities [19]. We tested the stability of our finite difference approximation by reducing the ODE solver tolerance and observing that the results of the sensitivity analysis converged the same values (results not shown). To approximate how the parameter influences model behavior we use ranked sensitivities R_j, defined as the two-norm over each column of S

$$R_j = \left(\sum_{i=1}^{N} S_{ij}^2 \right)^{1/2}.$$

3.2. Subset selection: Structured correlation analysis

The model considered here has inherent parameter interactions that necessitate the need for selecting parameter subsets with minimal unidentifiable parameter interactions. While various subset selection algorithms exist (e.g. [67]), we employ the structured correlation method by Ottesen et al. [68] to construct a set of identifiable model parameters. According to this method, a pair of parameters with a large correlation (and strongly coupled uncertainty) cannot both be uniquely estimated. This method systematically removes the least sensitive correlated parameters until an identifiable set remains. The input to this method is the sensitivity matrix - which means that any correlation is only valid within some neighborhood of the parameter values used to construct the sensitivity matrix.

Using the sensitivity matrix S in (14), the covariance matrix Γ is given by the inverse of the Fisher Information Matrix (FIM)

$$\Gamma = \mathsf{F}^{-1}, \tag{15}$$

where $F = \sigma^2 \mathsf{S}^T \mathsf{S}$. Note that F can only be inverted if S has full rank. Linearly dependent columns of S are a result of parameters being perfectly correlated, meaning that a parameter can be algebraically expressed in terms of other parameters. Additionally, columns of insensitive parameters ($R_j < h$) can lead to F having a large condition number and thus should be removed *a priori* from the sensitivity matrix input. The entries of Γ are used to compute the correlation matrix C with entries given by

$$\mathsf{C}_{i,j} = \frac{\Gamma_{i,j}}{\sqrt{\Gamma_{i,i}\Gamma_{j,j}}}.$$

C is a symmetric matrix with ones along the diagonal. Parameter pairs with a correlation value greater than γ (user defined threshold) are denoted correlated. Correlations between parameters show how the parameter values depend on each other when fitting experimental data from the same system.

3.3. Nonlinear least squares optimization: Levenberg-Marquardt

The goal of nonlinear least squares optimization is to estimate the set of parameters $\hat{\theta}$ that minimizes the difference between the model output $x(t, \theta)$ and the data y, assumed to be some function of the model output corrupted with additive noise; e.g.

$$y_i = g(x(t_i, \theta)) + \epsilon_i, \tag{16}$$

where y_i denotes the i'th data point, $x(t_i, \theta)$ the model response at the i'th time point, $g(\cdot)$ the observation function mapping the model variables to the measured states, and ϵ_i the normally distributed observation error. In this study, $g(\cdot)$ extracts the left ventricular volume and pressure time-series.

To fit our model to data, we use generalized nonlinear least squares to determine a parameter set $\hat{\theta}$, which minimizes the sum of squares cost function

$$J(\theta) = \sum_{k=1}^{2} J_k(\theta), \;\; J_k(\theta) = r_k^T r_k. \tag{17}$$

The residual vectors r_k are defined as

$$\begin{aligned} r_1 &= \frac{p_{\mathrm{lh,m}} - p_{\mathrm{lh,d}}}{\max(p_{\mathrm{lh,d}})} \quad \text{and} \\ r_2 &= \frac{V_{\mathrm{lh,m}} - V_{\mathrm{lh,d}}}{\max(V_{\mathrm{lh,d}}) - \min(V_{\mathrm{lh,u}})}. \end{aligned} \tag{18}$$

The subscripts "m" and "d" denote the model and data, respectively. Dividing the residuals by the amplitude of the data ensures that the optimization procedure gives equal weight to both model outputs.

To estimate $\hat{\theta}$ we employ the Levenberg–Marquardt optimization routine by Kelley [69]. To obtain a well scaled problem, we estimate the natural log of the true parameter values. As part of the optimization routine we discard parameter values that are 20 times larger or smaller than the nominal estimate. Like other gradient based optimization routines, the choice of the initial parameter vector θ_0 is important. If the cost function has multiple minima the optimization routine may end in an undesirable or unrealistic local minimum. Using the physiologically-justified nominal parameter values described in Section 2.3 helps to place our θ_0 closer to a physiologically realistic minimum. To verify that the optimization converged we randomly perturbed the nominal values by 10% and observed that the parameters all converged to the same values.

3.4. Uncertainty quantification

Uncertainty quantification (UQ) is the process of determining uncertainties in estimated model parameters given uncertainties in the model formulation and experimental measurements (the inverse problem), as well as establishing how uncertainties in model inputs (such as parameters) affect the model output (forward propagation of uncertainty). In this study, we utilize UQ procedures from both frequentist and Bayesian statistical frameworks. We calculate confidence intervals and Bayesian credible intervals to measure the precision of the model in predicting the mean response. These approaches are outlined below; for more details, see [70].

3.4.1. Frequentist approach

Frequentist uncertainty propagation methods are computationally inexpensive compared to their Bayesian analog. Most frequentist statistics are derived from asymptotic assumptions assuming that the uncertainty distributions take a Gaussian shape, whereas Bayesian methods make no assumption about the shape of the underlying distributions. One of the main benefits of the asymptotic assumptions is that uncertainty distributions can be expressed as explicit formulas in the frequentist perspective. Frequentist confidence intervals can be calculated from

$$\hat{y}_i \pm t_{N-p}^{\alpha/2} s (g_i^T (\mathbf{S}^T \mathbf{S})^{-1} g_i)^{1/2}, \tag{19}$$

where $t_{N-p}^{\alpha/2}$ is the student t-distribution with $N - p$ degrees of freedom (N is the number of data points and p is the number of parameters), s is the estimate of the model standard deviation σ, S is the sensitivity matrix, and g_i is the i'th row of S stacked as a column vector. Frequentist prediction intervals can be calculated in a similar manner by

$$\hat{y}_i \pm t_{N-p}^{\alpha/2} s (1 + g_i^T (\mathbf{S}^T \mathbf{S})^{-1} g_i)^{1/2}. \tag{20}$$

3.4.2. Bayesian approach: Delayed rejection adaptive metropolis (DRAM)

While frequentist methodology is fundamentally rooted in quantifying uncertainty in terms of repeating the data generating procedure, Bayesian inference is conditioned on a single data set; this allows for uncertainty about parameters to be expressed by probability distributions. In the Bayesian framework, θ represents a vector of random variables. Given observations $y = \{y_1, ..., y_n\}$, Bayes' formula

$$\pi(\theta|y) = \frac{\pi(y|\theta)\pi(\theta)}{\pi(y)} \tag{21}$$

describes how the posterior density $\pi(\theta|y)$ relates to the prior density $\pi(\theta)$, encompassing any *a priori* information known about the parameters, and the likelihood $\pi(y|\theta)$ of observing the data y for the model given θ. The marginal density $\pi(y)$ of the data typically functions as a normalization factor and can be determined by

$$\pi(y) = \int \pi\left(y \middle| \pi\right) \pi(\theta)\, d\theta. \tag{22}$$

Under the hypothesis (16), the likelihood function is given by

$$\pi_k(y|\theta) = \frac{e^{-J_k(\theta)/2\sigma_k^2}}{(2\pi\sigma^2)^{n/2}}, \tag{23}$$

where $J_k(\theta)$ denotes the least square cost defined by (17), n is the number of data points, and σ_k^2 is the model variance - the k index denotes the variance for pressure ($k = 1$) or volume ($k = 2$). Both σ_1^2 and σ_2^2 are parameters represented by probability distributions that are also estimated. With a known likelihood and prior density $\pi_k(\theta)$, it is possible to estimate the posterior density $\pi(\theta|y)$ if the integral (22) in the normalizing constant can be estimated. While this route is possible, the evaluation of high-dimensional integrals is a difficult and expensive, and is currently an active area of research; see, e.g., sparse grid methods [71,72] and quasi-Monte Carlo methods [73,74].

An alternative is to use Monte Carlo integration to randomly sample from the density $\pi(y|\theta)\pi(\theta)$. Many suitable Markov chain Monte Carlo (MCMC) methods exist in the literature (see [75] for an overview). This study uses the DRAM algorithm [36], which combines two methods for improving efficiency of Metropolis-Hastings type MCMC algorithms: delayed rejection (DR) [76] and adaptive Metropolis (AM) [77]. These Metropolis-type methods are acceptance-rejection algorithms that accept new parameter samples only if the likelihood of the new candidate is higher than the current sample. DR allows for additional proposals per step if the initially proposed step is not accepted, thereby increasing the acceptance rate and well-mixing of the sample. AM allows for updating of the covariance matrix based on the history of the sample, thereby helping the algorithm to make better proposals and move toward the correct posterior distribution faster, reducing the burn-in period.

We use (23) as our likelihood distribution, uninformed diffuse Gaussian distributions centered around the optimized point estimate from Section 3.3 as our prior distribution, and a Gaussian proposal distribution. To ensure a well scaled problem we have DRAM estimate the natural log of the true parameter densities like we do Section 3.3. Samples are taken from the DRAM-estimated parameter probability distributions to compute Bayesian credible and prediction intervals; for more details, see [36,70]. In this study, we utilize the MCMC toolbox by Haario et al. (2006) at http://helios.fmi.fi/~lainema/mcmc/, which includes code for running DRAM as well as for computing Bayesian credible and prediction intervals.

4. Results

In this section, we use the step-by-step procedure described in Section 3 to systematically estimate an identifiable subset of parameters for the cardiovascular compartment model derived in Section 2.2 that fit left ventricular volume and blood pressure data described in Section 2.1.

4.1. Nominal parameter values

Given that sensitivity and subset selection analysis are determined at an estimate of the local minimum, the first step involves using available data and literature to determine the best possible nominal parameter values, as described in Section 2.3. Second, we manually shift the starting point of the data so the model predictions and data both begin at the same point of the cardiac cycle, as shown in Fig. 5(a) and described in Section 3. This estimate of the data shift is refined in a later model optimization step.

4.2. Sensitivity analysis and subset selection

Next, we employ local sensitivity analysis and structured correlation, along with physiological knowledge, to construct a subset of identifiable model parameters.

Fig. 6 depicts normalized ranked parameter sensitivities and the subset of identifiable parameters (24) for all three animals. Ranking the parameters by sensitivity provides initial insight into what parameters are most influential in determining model behavior. Note that the ranked sensitivities of parameters R_A and E_{sa} are orders of magnitude smaller than the other parameters, thus these parameters were removed *a priori* from the set of parameters analyzed. We used the structured correlation algorithm from Section 3.2 to obtain an identifiable parameter set. For all three rats we used a correlation threshold $\gamma = 0.85$ as an upper bound on the pairwise correlations between parameters.

This allowed us to construct a multitude of putative parameter subsets and organizes them into a correlation tree (results not included; see [78] for an example of a correlation tree produced by structured correlation analysis). We screened these putative subsets by individually optimizing them and checked if (1) the optimized values were not hitting their upper/lower bounds, (2) the resulting fit to data was qualitatively good, and (3) the model solutions for the non-left ventricle compartments were physiologically realistic.

Since no data are available to distinguish the two compartments on the arterial and venous side it is not possible to separate dynamics between compartments, to avoid inconsistency we fixed parameters for the smaller arterial and venous compartments (la) and (lv) (E_{la} (insensitive), E_{lv}, R_A (insensitive), and R_v). Covariance analysis of remaining parameters $\tilde{\theta} = \{R_S, E_{sa}, E_{sv}, T_S, T_R, E_m, E_M\}$ revealed that:

- Parameters (E_{sa}, E_m) and (E_{sv}, E_m) are correlated. Of these E_{sa} is the least sensitive, so we fixed this parameter at its nominal value.

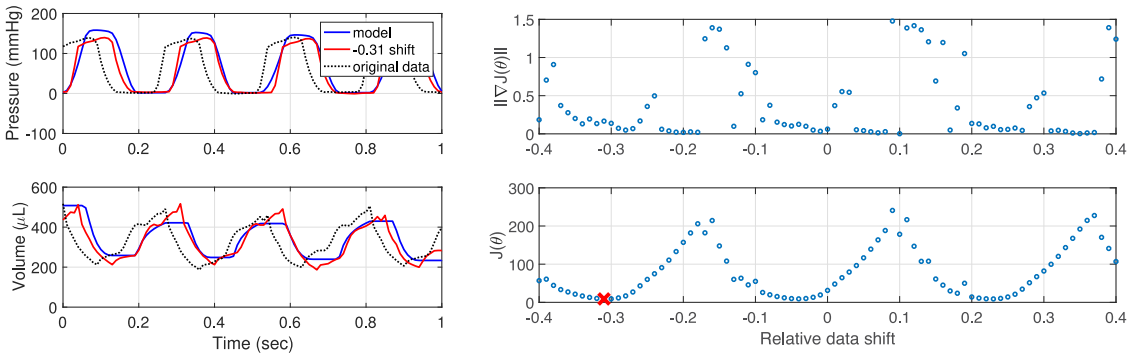

Fig. 5. (a) Manual shifting of the data starting point for Rat 1. The blue curve is the model solved using nominal parameters, the dotted curve is the original phase of the data, and the red curve is the same data shifted 0.24 s to the right in order align the phase of the model and data. Manual shifting for Rat 2 and 3 data sets are similar. (b) Determining the optimal data shift for Rat 1. The top plot shows the value of the gradient and the bottom plot shows the value of the cost function (17) as a function of relative data shifts. The red "x" in the bottom plot denotes the smallest value of the cost function and our optimal data shift. Results for Rat 2 and 3 show a similar pattern. (For interpretation of the references to color in this figure legend, the reader is referred to the web version of this article.)

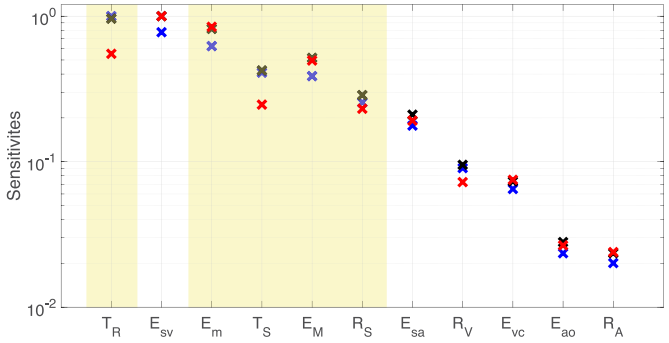

Fig. 6. Ranked parameter sensitivities. Blue, black, and red x's indicate relative sensitivities of Rats 1, 2, and 3 respectively. Yellow highlighted regions indicate parameters included in the subset (24). (For interpretation of the references to color in this figure legend, the reader is referred to the web version of this article.)

- Parameters E_{sv} and E_m are correlated and have similar sensitivity. Both parameters determine venous filling and given data are available in the left ventricle, we chose to fix E_{sv} while estimating E_m.

In summary, the resulting parameter subset is

$$\theta = \{R_S,\ T_S,\ T_R,\ E_m,\ E_M\}. \tag{24}$$

4.3. Optimization

Using the nominal parameters given in Table 3, we estiamte the parameter subset (24) using a Levenberg-Marquardt optimization scheme; we tested convergence of the optimizer by varying the initial guess around the nominal values. Results were verified by randomly perturbing the nominal values by 10% and optimizing the perturbed parameters. For ten unique perturbations, all of the parameters converged to the same values (results not included). To ensure that the solution has settled to steady state, computations were done over entire 20 s of data, with the least squares cost evaluated over the last 0.5 s of the data shown in Fig. 1. As part of the optimization procedure we also estimate the data shift, using nominal value estimated manually as described in step 1. This was done by repeating optimizations for a large number of shifts. Results showed (5(b)) that there are multiple parabolic minimums for the cost reflecting the pulsatile nature of cardiovascular mechanics. We chose the minima that provided the smallest cost (17). Results depicted in Fig. 5 shows the cost (17) and gradient plotted as a function of relative data shifts for Rat 1 (similar results were obtained for rats 2 and 3).

Optimization results for all three rats, with optimal shifts, are reported in Table 3 listing the nominal and optimized parameter values, and Fig. 7 shows the model fit with optimized parameter values compared to the data. Note that we report the true parameter values and not the natural log of the parameters used by the Levenberg–Marquardt optimizer.

Table 3
Model parameter values for each rat. For each entry (a,b,c) corresponds to Rat 1, 2, and 3, respectively. Bolded parameters are those included in subset (24) and estimated using Levenberg–Marquardt optimization and DRAM. Reported DRAM values are the means of the resulting parameter sample chains with the 10,000 sample burn-in removed.

Parameter	Units	Nominal ($\cdot 10^{-1}$)	Lev-Mar ($\cdot 10^{-1}$)	DRAM Mean ($\cdot 10^{-1}$)
R_A	s mmHg/μl	0.011, 0.014, 0.012	–	–
R_S	s mmHg/μl	0.942, 1.155, 1.003	1.600, 1.630, 2.196	1.588, 1.631, 2.187
R_V	s mmHg/μl	0.002, 0.001, 0.002	–	–
E_{la}	μl/mmHg	9.641, 8.446, 8.535	–	–
E_{sa}	μl/mmHg	1.193, 1.045, 1.056	–	–
E_{sv}	μl/mmHg	0.006, 0.003, 0.006	–	–
E_{lv}	μl/mmHg	0.050, 0.027, 0.049	–	–
T_S	s	2.500, 2.500, 2.500	4.544, 4.161, 4.166	4.518, 4.163, 4.213
T_R	s	6.000, 6.000, 6.000	7.309, 6.409, 8.149	7.403, 6.409, 8.161
E_m	mmHg/μl	0.043, 0.026, 0.042	0.050, 0.025, 0.039	0.049, 0.025, 0.039
E_M	mmHg/μl	5.476, 3.864, 2.595	5.965, 4.366, 3.252	5.904, 4.364, 3.254

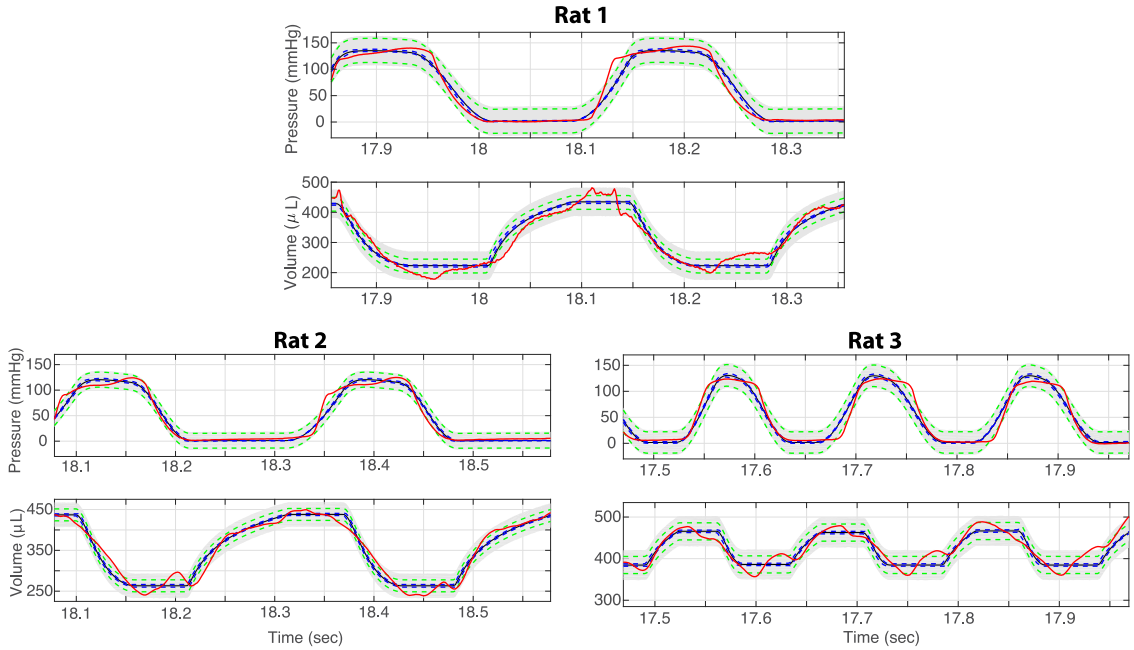

Fig. 7. Optimization and uncertainty propagation results for all three rats. The red curve is the data, the blue dotted lines show the frequentist confidence interval (19), and the green dashed lines show the frequentist prediction interval (20). The black line is the model evaluated with the means of the DRAM estimated parameter densities, the dark grey band (too narrow to be seen in this figure) is the Bayesian credible interval, and the light grey band is the Bayesian prediction interval. (For interpretation of the references to color in this figure legend, the reader is referred to the web version of this article.)

4.4. Uncertainty quantification

The point-estimates obtained using the Levenberg–Marquart routine were used to initialize both frequentist and Bayesian UQ methods, to construct confidence and credibility intervals along with prediction intervals for the model output predictions. This choice was motivated by the need to minimize the high computational cost of solving stiff ODEs. To demonstrate that our workflow is reproducible across data sets we repeated computations for all three data sets shown in Fig. 1.

To perform UQ, we considered both the frequentist formulas stated in Section 3.4.1 and the Bayesian inference using DRAM as described in Section 3.4.2. Using the optimized values, we applied Eqs. (19) and (20) to compute frequentist confidence and prediction intervals, respectively. The optimized point estimates were used to construct the prior distribution of parameters as diffuse Gaussian distributions (uninformed prior centered around the optimized point estimate) for the DRAM algorithm. This choice of a prior is justified by the fact that we had no additional information to construct a more informative prior distribution. Chains of 100,000 sample points were generated using DRAM. Fig. 8 shows the resulting DRAM-estimated parameter chains, parameter densities, and pairwise parameter correlations for rat 1, similar results were obtained for the other animals. Frequentist UQ intervals were computed from Eqs. (19) and (20), and Bayesian UQ intervals were constructed by solving the model over randomly sampled values from the posterior parameter chains. Fig. 7 compares the resulting frequentist and Bayesian UQ for all three animals.

5. Discussion

It is well known that blood vessels dilate and constrict to maintain homeostatic levels of blood flow and pressure. However it is challenging to quantify the functionality of the heart and vasculature. Cardiovascular quantities including volumes, flows, and pressures (e.g. ventricular volume and pressure - studied here) can be measured experimentally, yet the system properties that underlies specific outputs can typically not be measured directly, e.g. peripheral vascular resistance, vessel compliance, or cardiac contractility. The simple cardiovascular model presented here was chosen to illustrate a workflow associated with designing and validating the model components, including (1) model formulation, (2) sensitivity analysis and subset selection, (3) optimization, and (4) uncertainty quantification. Below we discuss each step and summarizing major findings.

Model Formulation and nominal parameter values. The model type used here is not new, and even though previous studies, e.g. [79–82] involve more complex interactions (e.g. nonlinear venous compliance, systemic and pulmonary sub-circuits, inductors, etc.), the important conclusion is that to obtain reliable parameter estimates it is essential to compute nominal parameters that are physiologically reasonable. This allows us to determine what parameters are identifiable and to assess model uncertainty. The specific model discussed here includes measurements of left ventricular volume and pressure. Other commonly available data include measurements of arterial pressure, central venous pressure, and cardiac output. For most studies, including the one presented here, assumptions must be made since not all information is available, e.g. we used literature estimate to determine the unstressed volume fraction. This is a quantity that is important, but as discussed by Spiegel [83], no good experimental method exists for determining the stressed-to-unstressed ratio. The model presented here was fitted to left ventricular pressure and volume, the advantage being that both arterial and venous pressures and stroke volume can be determined, while aortic pulse pressure had to be estimated. Many other studies, e.g. the study by Williams et al. [15] rely on non-invasive measurements typically only available at the arterial side. To identify reliable parameters this model can only be done by incorporating assumptions about venous pressure and cardiac output. As discussed in the study by Pironet et al. [26] reliable parameter estimates require measurements of both pressures and left ventricular stroke volume. In general, we show how to determine a subset of identifiable parameters that can be estimated by fitting model output to data.

The model and data analyzed here are pulsatile. To accurately fit

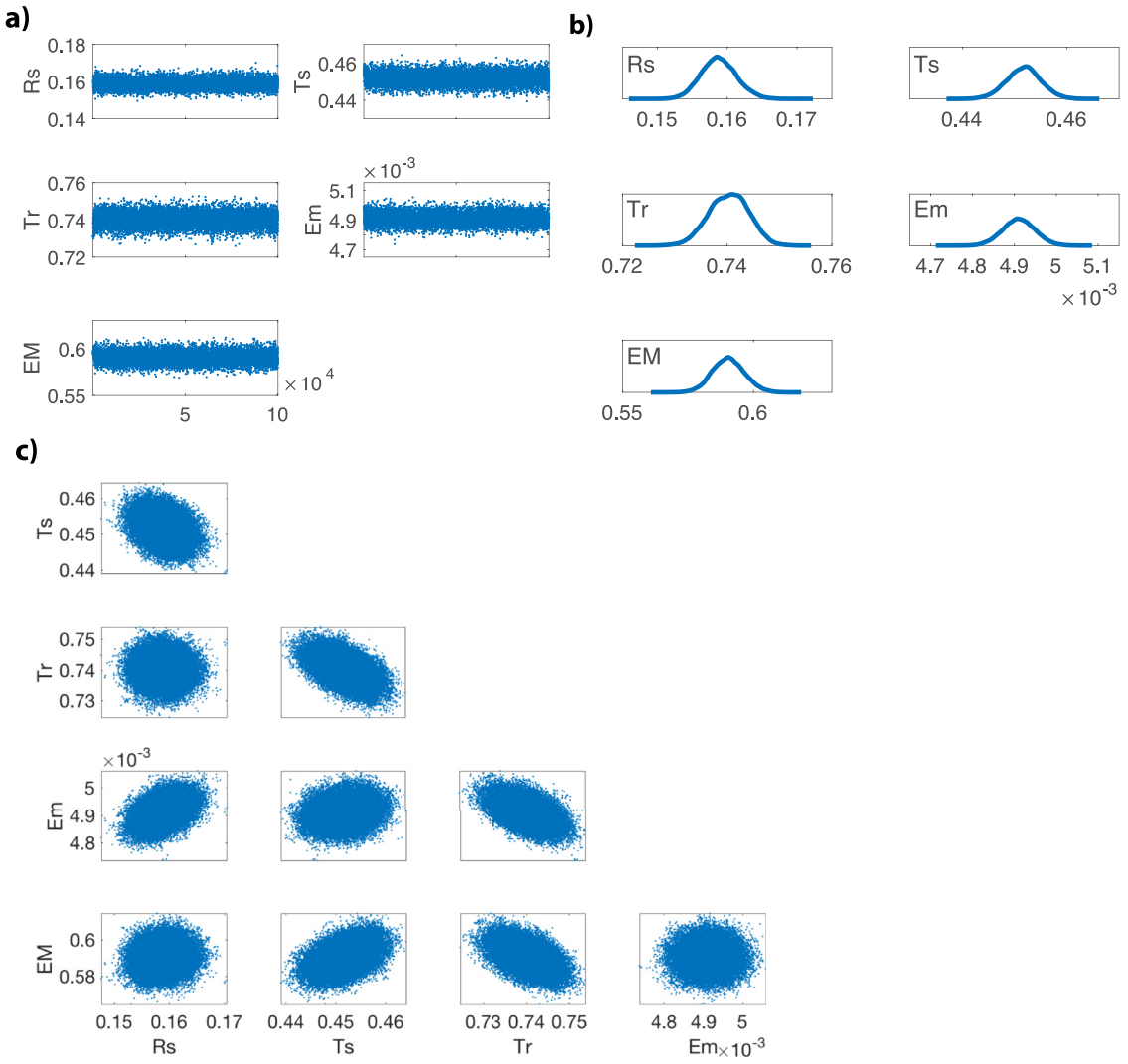

Fig. 8. MCMC diagnostics from DRAM for Rat 1. **(a)** Parameter chains of subset (24) using DRAM with 100,000 sample points. The first 10,000 samples are considered as the burn-in period and are not used in computing the resulting parameter densities or Bayesian UQ. **(b)** Parameter densities of subset (24). **(c)** Pairwise correlations of the resulting parameter densities from DRAM. Each plot can be interpreted as a marginal density by integrating over all of the other parameters not contained in the respective plot. Results for Rats 2 and 3 are similar.

model to data in the case of this periodic cardiovascular systems model it is essential to align the phase of the periodic driving function with that of the data. The phase of model predictions is determined by initial conditions. Since for most compartments only either mean and/or minimum or maximum predictions are available it is difficult to set up initial conditions that provide precise alignment of model predictions to data. Mathematically, we want to initialize the model at "steady state," so that with constant periodic forcing the solution oscillates around a known mean. Depending on time-scale of the model, typically dictated by compartment elastance, computations should be done over a long enough time to allow the system to reach a steady state. Once steady state is achieved, we show how to systematically determine the optimal shift of the data best aligning the model predictions with the data. To our knowledge this element has not been addressed in previous studies with respect to cardiovascular models.

Finally, the pulsatile nature of this model is facilitated by periodic forcing of the system combined with valves. This model uses diodes to predict flow into and out of the valves, while this is the most typical formulation [26,84], the discrete opening and closing of valves make the system of differential equations stiff. While the diodes approach is easier to formulate, it introduces a discontinuity in the system of equations not characteristic of the pressure-dependent resistances [15] or valves accounting for inertia [8,85,86]. Even when accounting for inertia, the system of ODEs arising in pulsatile cardiovascular models is stiff and requires careful attention when solving numerically; for more details on solving stiff differential equations, see, e.g. [87,88].

Below we discuss results of each component of our step-by-step approach engaged to estimate identifiable parameters and determine model uncertainty.

Sensitivity analysis and subset selection. Most cardiovascular models, as the one formulated here, are over-parameterized compared to available data. While data available for parameter estimation often is dense in time, only a few states are measured, e.g. the model presented here are based on predictions of left ventricular volume and pressure. Therefore, care must be taken both in the model building phase, by not including more compartments than can be justified, and in the parameter estimation phase, only estimating identifiable parameters. The first step in the analysis phase involves sensitivity analysis. There are many methodologies to consider, and care must be taken since the system of equations often is nonlinear and stiff. For this study we elected to calculate sensitivities using a forward difference methodology, that we validated by reducing our ODE solver tolerance and observing that the results converged to stable values. While this

approach is easy, more effort could be put into study the system globally, e.g. using Sobol indices or Morris screening [29,89]. Alternatively, local results could be obtained by solving sensitivity equations in the complex plane [90] - however this method requires that model be analytic and the diode valve formulation we employ violates this condition.

Parameters were ranked from most to least sensitive using a two-norm averaging over the part of the data used for model validation (i.e. after steady oscillations have been achieved, when the effects of initial conditions disappear). Given the periodic nature of the model studied here this approach makes sense, yet for other model types, generalized sensitivity [91] may be more appropriate as they also provide information about what part of the data specific parameters influence.

Results of our sensitivity analysis revealed that R_V, E_{sv}, E_{la}, and R_A were insensitive compared to the other parameters, as a result we chose to keep those fixed at their nominal values. Another use of sensitivities is to detect if specific model components can be eliminated or should be described in more detail. It should be noted that the sensitives we use reflect how an individual parameter influences the proximity of the model solution to the data rather than providing a metric of how it influences the model behavior.

One can observe that four out of the five parameters in the identifiable subset (24) are used to define the time-varying elastance function (5). This result is not particularly surprising, as our data set is completely contained within the left ventricle compartment of the model. It is essential to understand the identifiability of a parameter is highly dependent upon the type of the data used. For example, this study could be repeated using a more commonly available data set such as central arterial pressure (corresponding to the large artery compartment of the model) rather left ventricular data. It is conceivable that parameters R_A and E_{la} would very sensitive to this data set and likely be contained within the identifiable subset from the structural correlation analysis. Depending on the availability of data and one's modeling objectives, subset selection results could be used to inform model development and refinement. For the left ventricular pressure and volume data used in this study, a simpler three compartment model could potentially be used to obtain the same quality of fit.

Parameters being sensitive do not equate to being identifiable [67,78]. Our results demonstrate this phenomena by the fact the highly sensitive parameter E_{sv} is not part of the identifiable subset (24). Physiologically, the high sensitivity of E_{sv} makes sense - stiffness of the veins directly influences venous return to the heart and thus diastolic filling. However, including E_{sv} in the subset of parameters to optimize often resulted in parameters hitting their upper or lower bounds (results not included). This indicates the parameters bounds are either too narrow, or the subset is unidentifiable. When implementing the structured correlation analysis in Section 3.2 one initially constructs a multitude of putative parameter subsets and organizes them into a correlation tree (see [78] for an example of a correlation tree). We screened these putative subsets by individually optimizing them and checked to see if the (1) optimized values were not hitting their upper/lower bounds, (2) the resulting fit to data was qualitatively good, and (3) the model solutions for the non-left ventricle compartments were physiologically realistic. For example, one of the candidate subsets we screened was $\{R_S, E_{sv}, T_S, T_R, E_M\}$. This subset satisfied two of these criterion (optimized parameters did not hit upper/lower bounds, and the fit to data was qualitatively good), however it the model solution with this optimized subset produced a hypertensive pulse pressure in the large and small artery compartments (140/120 mmHg). The subset (24) was the only one that satisfied all three of these criterion. Thus it is important to combine sensitivity analysis with identifiability analysis, or subset selection (the term used here) to identify relationships among parameters. However, determining if a specific parameter interaction is identifiable is nontrivial. Pironet et al. [26] illustrated that elastance and resistance parameters form a structurally identifiable relationship given left ventricular stroke volume and pressure data for every compartment in their model. Their model uses a simplified elastance driving function with no parameters and assumed that stroke volume and all compartment pressures were available. Consequently results from the Pironet model cannot directly be translated to our model. Mahdi et al. [23] provided some guidelines for constructing arbitrarily complex structurally identifiable spring-dashpot networks, however their results were constrained to linear viscoelastic formulations. Our workflow is motivated by analyzing the practically identifiable components of cardiovascular models to make predictive inference through the use of uncertainty quantification.

Intuitively one would expect that parameter interactions hinder the identifiability of a model. However it is crucial to understand, even though intimately related, that correlation and identifiability are distinct concepts. Correlation refers to the precise structure and relationship between interacting parameters, whereas identifiability refers to mapping between the parameter space and the model output, which ideally would be one-to-one. So while minimizing parameter interactions and correlations can be an effective strategy to find an identifiable subset of parameters, it is not an exhaustive or universally applicable strategy for any arbitrary model. We found that approaching the parameter estimation problem from a Bayesian perspective was particularly useful in this regard as it allows one to visualize parameter interactions. It should also be noted that the ideal subset of "identifiable" parameters is highly dependent on the type of data available (e.g. pressure in large systemic arteries rather vs. the left ventricle) and may vary across individuals.

For this study we chose to use structural correlation analysis [67,78], which is local in nature and it only provides a first order approximation of the parameter correlations, i.e. it is not able to capture nonlinear parameter interactions. However, with good initial parameter estimates, this methodology has been shown to work [67,78,89]. In this study, we leverage this limitation using DRAM to estimate the parameters in a Bayesian framework. By representing the parameters as random variables, we can trace the exact shape of the joint densities and can visualize the parameter interactions, as shown in Fig. 8. Unidentifiable parameter subsets typically take more MCMC iterations to converge and often have more correlation in their pairwise density plots. We have illustrated that in Fig. 10 (using a slightly altered subset including $\theta = \{R_S, T_S, T_R, E_{sa}, E_m, E_M\}$, a subset that structured correlation analysis method determined correlated). Results demonstrate very mild correlations between E_M, E_m, T_S and T_R despite the subset (24) being identifiable. Our recommendation is to combine Bayesian parameter estimation techniques together with asymptotic subset selection methods in an iterative process to refine ones understanding of different model parameterizations and potentially find a practically identifiable subset of parameters.

Optimization. Similar to numerous other studies, e.g. [19], we used a nonlinear least squares methodology to obtain point-estimates for the identifiable parameters. This approach is commonly used for ODE models and data describing the kinetics and/or dynamics of a system [92]. There are many different styles of optimization algorithms with corresponding benefits and limitations. Gradient-based optimization methods such as Levenberg–Marquart are limited in that they do not search the entire the parameter space while minimizing the cost function. They are designed to find the nearest local minimum relative to the initial parameter estimate, rather than the global minimum. Other optimization routines that do explore the entirety of the parameter space could have been employed (e.g. Nelder–Mead, SPQ algorithm, or interior point optimization), but for well conditioned problems Levenberg–Marquart is computationally very efficient. As a result we put significant effort into *a priori* parameterization of the model to yield a well conditioned optimization problem, a topic we have not seen addressed in many cardiovascular models.

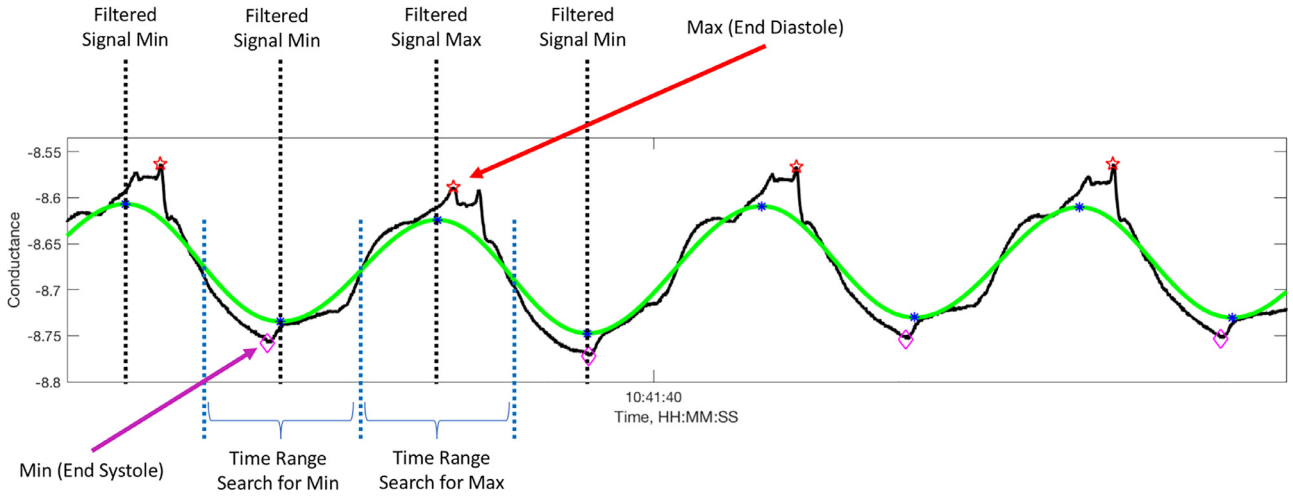

Fig. 9. Protocol for identifying minima (magenta diamonds) and maxima (red stars) of the raw conductance signal (measured as a voltage). The procedure for this is outline above where a filtered signal is used to define brackets of time to search over for minima and maxima. These values are averaged for all cycles in the baseline time course and then used to determine the conductance voltage that represents the end diastolic volume and the average difference between minimum and maximum that represents stroke volume. (For interpretation of the references to color in this figure legend, the reader is referred to the web version of this article.)

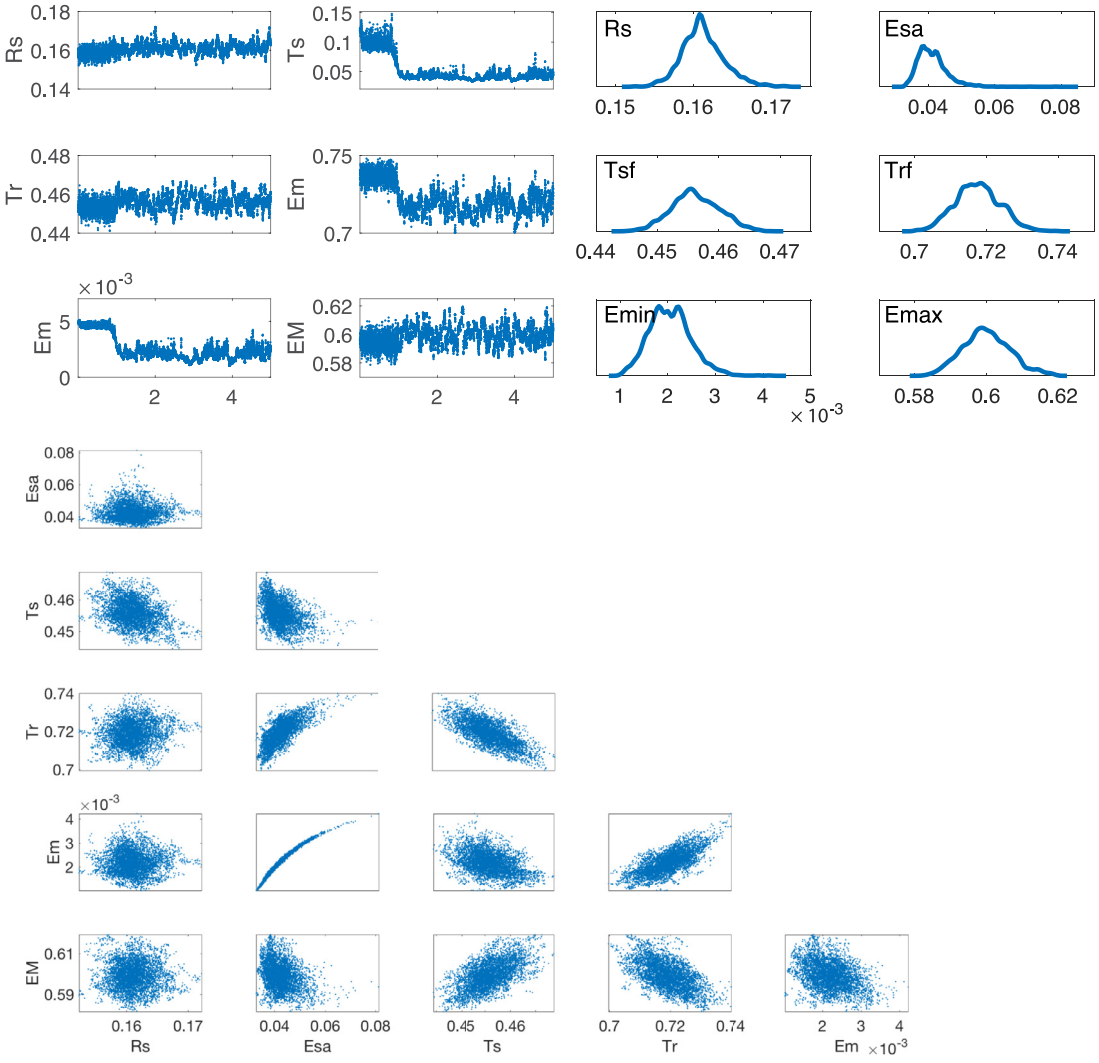

Fig. 10. Parameter densities of an unidentifiable subset. Posterior parameter chains were computed using 100,000 iterations of DRAM, with the first 10,000 iterations removed as burn-in.

Uncertainty Quantification. Having a high-quality model fit is rarely the end of one's modeling efforts. In particular if the model is to be adapted for analysis of clinical data it is essential to assess the limitations of a model's predictive power. This study used asymptotic and Bayesian methods to determine confidence, prediction and credible intervals. The field of uncertainty quantification is an active area of research [29,35,93–96] - these references are but a few examples of recent studies applying UQ to models of cardiovascular mechanics. For the utility that UQ promises, the obvious problem that has been neglected with regard effective implementation is that most methods assume that the mapping from the parameter space to the model output is one-to-one. This is a non-trivial condition that few models satisfy. Furthermore, very few studies have reported results of identifiability analysis prior to the implementation of the UQ procedure. While one can forcibly propagate the uncertainties of unidentifiable model inputs (parameters and/or data) through a model to obtain uncertainty bounds, the reproducibility and stability of such results are suspect.

Our analysis, utilizing the estimated subset of identifiable parameters (24) has allowed us to use both frequentist and Bayesian uncertainty propagation methods to achieve interpretable and tight uncertainty bounds around our model solutions. As a result of using a practically identifiable subset of parameters, our UQ bounds are reproducible and stable across distinct data sets. Results of analysis showed that asymptotic prediction intervals and the Bayesian prediction intervals are almost identical for pressure data, whereas prediction intervals are slightly wider for the volume data, the latter is likely a result of a higher noise level in the volume data than the pressure data.

Due to its flexibility in representing parameters as random variables, an advantage of the Bayesian framework is that UQ is an intrinsic feature. Assuming the model is identifiable and that the parameter chains have converged, credible and prediction intervals can be obtained by extracting model evaluations from the parameter chains. These uncertainty bounds are not subject to any potentially limiting assumption about their distribution, as their frequentist analogs are. The largest limitation to MCMC-type Bayesian approaches is the sheer computational cost. MCMC methods are robust, yet they require thousands of model evaluations to construct a converged posterior parameter distribution. For sufficiently complex models, MCMC may be an impractical route. As an alternative, sequential Bayesian methods such as particle filtering [97–100] or ensemble Kalman filtering [101–104] may reduce computational time by evaluating the model from one data point to the next, as opposed to integrating over the entire data set at once. Another option is to use model emulation within the DRAM evaluation [105]. For the cardiovascular model presented here, we can see in Fig. 7 that there is very little appreciable difference between the employed statistical approaches. Thus for future studies using this model and corresponding data sets, frequentist UQ alone may be sufficient.

In conclusion, we developed a model and estimated subject specific nominal parameters using available data and literature. We used local sensitivity analysis and subset selection to determine a set of identifiable parameters that were optimized against left ventricular pressure and volume data from three rats. Subsequently we used asymptotic and Bayesian analysis to estimate prediction and credible intervals, which since done in a close neighborhood of the optimal values were comparable. Given the computational cost associated with Bayesian methods, we propose to identify possible subsets and conduct estimations using both local and Bayesian approaches for a few test animals and then carry out larger population studies using only local methods.

Summary. In summary, our step-by-step approach showed that by removing parameter interactions by means of local sensitivity and structured correlation analysis, we can obtain the same subset of practically identifiable model parameters for all three rats. We used nonlinear least squares optimization to estimate this subset of parameters to provide a high quality fit to the data. Finally, we used both frequentist and Bayesian UQ methods to predict confidence, credibility and prediction intervals around the model output. The approached discussed here was demonstrated on a simple cardiovascular model, yet it is applicable to any model with data that can be formulated as a system of ODEs.

Appendix

Volume-conductance calibration procedure

The baseline pressure and volume time series data used in this study was extracted from a blood withdrawal experiment. These blood withdrawals preclude the typical conductance-volume calibration by use of Baan's equation. The following procedure is used to identify the maximal and minimal conductances (corresponding to end-diastole and end-systole respectively) for each cardiac cycle. The empirical curves (1) from our metadata analysis in Fig. 2 provide reference end-diastolic and stoke volumes as a function of body weight. These reference values are used to convert the raw conductance signal (recorded in volts) to volume.

1. The raw voltage signal of a selected approximately 20 s segment at baseline is first smoothed using a low pass filter.
2. This filtered signal is used to estimate the times associated with the maximal and minimal voltages.
3. Successive maximum and minimum voltage times are then averaged to estimate times halfway between maximum and minimum voltage. These times establish a time range to search the original raw voltage signal for maximum and minimum voltages. See Fig. 9.
4. The maximal and minimal voltages of the original raw voltage signal are now found for each heartbeat of the baseline data and then an average of all maximal voltages is taken along with an average of all minimal voltages. These maximal voltages can be attributed to the end diastolic volumes at baseline and the difference between the maximal and minimal voltages can be attributed to the stroke volumes at baseline.
5. Using Eq. (1), the relationships determined for left ventricular end diastolic volume and stroke volume as a function of body weight from our metadata analysis in Fig. 2, we can estimate these end diastolic volumes and stroke volumes for each animal in the study.
6. The volume as a function of voltage at baseline can now be determined using the average left ventricular end diastolic and stroke voltages and the estimated volumes from (1) by

$$V(t) = SV_{\text{ref}}\left(\frac{G(t) - G_{\text{ES}}}{G_{\text{ED}} - G_{\text{ES}}}\right) + (EDV_{\text{ref}} - SV_{\text{ref}}),$$

where $G(t)$ is the raw conductance signal, G_{ED} and G_{ES} are the averaged conductances corresponding to end-diastole and and end-systole, and EDV_{ref} and SV_{ref} are the reference end-diastolic and stroke volumes predicted by (1), and $V(t)$ is the volume time course.

Model equations

The complete system of differential equations describing the rates of change of the compartments of the model analyzed in this study are given as follows:

$$\begin{aligned}
\frac{dV_{\mathrm{lh}}}{dt} &= q_{\mathrm{mv}} - q_{\mathrm{av}} \\
\frac{dV_{\mathrm{la}}}{dt} &= q_{\mathrm{av}} - \frac{E_{\mathrm{la}}V_{\mathrm{la}} - E_{\mathrm{sa}}V_{\mathrm{sa}}}{R_{\mathrm{A}}} \\
\frac{dV_{\mathrm{sa}}}{dt} &= \frac{E_{\mathrm{la}}V_{\mathrm{la}} - E_{\mathrm{sa}}V_{\mathrm{sa}}}{R_{\mathrm{A}}} - \frac{E_{\mathrm{sa}}V_{\mathrm{sa}} - E_{\mathrm{sv}}V_{\mathrm{sv}}}{R_{\mathrm{S}}} \\
\frac{dV_{\mathrm{sv}}}{dt} &= \frac{E_{\mathrm{sa}}V_{\mathrm{sa}} - E_{\mathrm{sv}}V_{\mathrm{sv}}}{R_{\mathrm{S}}} - \frac{E_{\mathrm{sv}}V_{\mathrm{sv}} - E_{\mathrm{lv}}V_{\mathrm{lv}}}{R_{\mathrm{V}}} \\
\frac{dV_{\mathrm{lv}}}{dt} &= \frac{E_{\mathrm{sv}}p_{\mathrm{sv}} - E_{\mathrm{lv}}V_{\mathrm{lv}}}{R_{\mathrm{V}}} - q_{\mathrm{mv}}
\end{aligned}$$

where

$$q_{\mathrm{av}} = \begin{cases} \dfrac{p_{\mathrm{lh}} - E_{\mathrm{la}}V_{\mathrm{la}}}{R_{\mathrm{av}}} & \text{if valve open } p_{\mathrm{lh}} > p_{\mathrm{la}} \\ 0 & \text{otherwise (valve closed),} \end{cases}$$

$$q_{\mathrm{mv}} = \begin{cases} \dfrac{E_{\mathrm{lv}}V_{\mathrm{lv}} - p_{\mathrm{lh}}}{R_{\mathrm{mv}}} & \text{if valve open } p_{\mathrm{lv}} > p_{\mathrm{lh}} \\ 0 & \text{otherwise (valve closed).} \end{cases}$$

and

$$p_{\mathrm{lh}} = E_{\mathrm{lh}}(t)V_{\mathrm{lh}},$$

$$E_{\mathrm{lh}}(t) = \begin{cases} E_{\mathrm{m}} + \dfrac{E_{\mathrm{M}} - E_{\mathrm{m}}}{2}(1 - \cos(\pi t/T_{\mathrm{S}})) & 0 < t < T_{\mathrm{S}} \\ E_{\mathrm{m}} + \dfrac{E_{\mathrm{M}} - E_{\mathrm{m}}}{2}\cos(\pi(t - T_{\mathrm{S}})/(T_{\mathrm{R}} - T_{\mathrm{S}})) & T_{\mathrm{S}} < t < T_{\mathrm{R}}, \\ E_{\mathrm{m}} & T_{\mathrm{R}} < t < T \end{cases}$$

Unidentifiable subset

Representing parameters as probability distributions can provide information about the identifiability of a multi-dimensional parameter distribution. Plots of parameter chains and densities such as those seen in Figs. 8 are the fundamental diagnostic tools to asses if the MCMC parameter optimizer has converged. The posterior parameter chain plot should ideally be white noise of the distribution, and the posterior parameter density should have a single clearly defined mean. Unidentifiable parameter distributions often have multi-modal distributions that can be observed from plots of the parameter chain and the density. One can interpret a multi-modal distribution as a parameter chain that has not converged, or an unidentifiable parameter. Should the first scenario be the case be, one can run the MCMC algorithm for more iterations until the distribution converges to the true posterior. However, if the converged parameter distribution is still multi-modal, it indicates that multiple values of a parameter can be used to produce the same model output. By definition, this means that the parameter is unidentifiable.

To illustrate how an unidentifiable subset of parameters can result in multimodal posterior parameter distribution we ran DRAM using a subset which included E_{sa}. Results from this simulation, shown in Fig. 10, revealed that it takes approximately 12,000 iterations for the parameter chains to burn-in (compared with the identifiable subset that start near the converged distribution), even with this long burn-in the chains are not well mixed. Poorly mixed parameter chains are indicative of an ill-conditioned optimization problem [106]. Further note that the parameter densities have lumpy shapes, e.g. parameters E_{sa} and E_{m} exhibit bimodality. Furthermore, we observe that E_{sa} and E_{m} have a highly correlated joint density. One may be able to run the MCMC routine for more iterations to get better mixed chains and smooth out the densities, but for an arbitrarily complex model it may not be worth the effort given the raw computational time and resources MCMC routines require. We note that while the modality of posterior parameter distributions can be used to assess the identifiability of a subset of parameters, an individual parameter exhibiting multi-modal behavior is not itself unidentifiable. From these results alone, we could not explicitly determine if E_{sa} or E_{m} are unidentifiable. Additionally, there are situations where a third parameter with a relatively smooth density may in fact be the unidentifiable culprit. The posterior parameter density is a joint-distribution of all the parameters, so any multi-modal behavior must be considered in the context of the other parameters in the distribution.

Supplementary material

Supplementary material associated with this article can be found, in the online version, at 10.1016/j.mbs.2018.07.001.

References

[1] L. Formaggia, A.M. Quarteroni, A. Veneziani (Eds.), Cardiovascular Mathematics: Modeling and Simulation of the Circulatory System, Springer, 2009.
[2] A.M. Quarteroni (Ed.), Modeling the Heart and the Circulatory System, Springer, 2015.
[3] F.N. Van de Vosse, N. Stergiopulos, Pulse wave propagation in the arterial tree, Ann. Rev. Fluid Mech. 43 (2011) 467–499.
[4] J.T. Ottesen, M.S. Olufsen, J.K. Larsen, Applied Mathematical Models in Human

Physiology, SIAM, 2004.
[5] J.T. Ottesen, V. Novak, M.S. Olufsen, Development of patient specific cardiovascular models predicting dynamics in response to orthostatic stress challenges, Mathematical Modeling and Validation in Physiology, Springer, 2013, pp. 177–213.
[6] P. Blanco, F. RA, A 3d-1d-0d computational model for the entire cardiovascular system, Mecánica Computacional 24 (2010) 5887–5911.
[7] I. Kokalari, T. Karaja, M. Guerrisi, Review on lumped parameter method for modeling the blood flow in systemic arteries, J. Biomed. Sci. Eng. 6 (2013) 92–99.
[8] S. Yubing, P. Lawford, R. Hose, Review of zero-d and 1-d models of blood flow in the cardiovascular system, Biomed. Eng. Online 10 (2011).
[9] F. Sotiropoulos, T.B. Le, A. Gilmanov, Fluid mechanics of heart valves and their replacements, Annu. Rev. Fluid Mech. 48 (2016) 259–283.
[10] Y. Hoi, H. Meng, S.H. Woodward, B.R. Bendok, R.A. Hanel, L.R. Guterman, L.N. Hopkins, Effects of arterial geometry on aneurysm growth: three-dimensional computational fluid dynamics study, J. Neurosurg. 101 (4) (2004) 676–681.
[11] U. Morbiducci, R. Ponzini, M. Grigioni, A. Redaelli, Helical flow as fluid dynamic signature for atherogenesis risk in aortocoronary bypass. a numeric study, J. Biomech. 40 (3) (2007) 519–534.
[12] D.A. Beard, K.H. Pettersen, B.E. Carlson, S.W. Omholt, S.M. Bugenhagen, A computational analysis of the long-term regulation of arterial pressure, F1000Res 2 (2013) 208.
[13] T.E. Dick, Y. Molkov, G. Nieman, Y.-H. Hsieh, F.J. Jacono, J. Doyle, J. Scheff, S.E. Calvano, I.P. Androulakis, G. An, et al., Linking inflammation, cardiorespiratory variability, and neural control in acute inflammation via computational modeling, Front Physiol. 3 (2012) 222.
[14] M.D. Thompson, D.A. Beard, Physiologically based pharmacokinetic tissue compartment model selection in drug development and risk assessment, J. Pharm. Sci. 101 (1) (2012) 424–435.
[15] N. Williams, O. Wind-Willassen, R. Program, J. Mehlsen, J. Ottesen, M. Olufsen, Patient-specific modelling of head-up tilt, Math. Med. Biol. 31 (2014) 365–392.
[16] M.L. Neal, J.B. Bassingthwaighte, Subject-specific model estimation of cardiac output and blood volume during hemorrhage, Cardiovasc. Eng. 7 (2007) 97–120.
[17] D. Zinemanas, R. Beyar, S. Sideman, Relating mechanics, blood flow and mass transport in the cardiac muscle, Int. J. Heat Mass Transf. 37 (1994) 191–205.
[18] M. Olufsen, J. Ottesen, H. Tran, L. Ellwein, L. Lipsitz, N. V, Blood pressure and blood flow variation during postural change from sitting to standing: model development and validation, J. Appl. Physiol. 99 (2005) 1523–1537.
[19] S. Pope, L. Ellwein, C. Zapata, V. Novak, C. Kelley, M. Olufsen, Estimation and identification of parameters in a lumped cerebrovascular model, Math. Biosci. Eng. 6 (2009) 93–115.
[20] J. Revie, D. Stevenson, J. Chase, C. Hann, B. Lambermont, A. Ghuysen, P. Kolh, G. Shaw, S. Heldmann, T. Desaive, Validation of subject-specific cardiovascular system models from porcine measurements, Comput. Meth. Prog. Biomed. 109 (2013) 197–210.
[21] P. Pacher, T. Nagayama, P. Mukhopadhyay, S. Bátkai, D.A. Kass, Measurement of cardiac function using pressure–volume conductance catheter technique in mice and rats, Nat. Protoc. 3 (2008) 1422.
[22] E.T. Mackenzie, J.K. Farrar, W. Fitch, D.I. Graham, P.C. Gregory, A.M. Harper, Effects of hemorrhagic hypotension on the cerebral circulation. i. cerebral blood flow and pial arteriolar caliber, Stroke 10 (1979) 711–718.
[23] A. Mahdi, N. Meshkat, S. Sullivant, Structural identifiability of viscoelastic mechanical systems, PLoS ONE 9 (2014) e86411.
[24] H. Miao, X. Xia, A.S. Perelson, H. Wu, On identifiability of nonlinear ode models and applications in viral dynamics, SIAM Rev. 53 (2011) 3–39.
[25] J. Kirk, M. Saccomani, S. Shroff, A priori identifiability analysis of cardiovascular models, Cadiovasc. Eng. Technol. 4 (2013) 500–512.
[26] A. Pironet, P. Dauby, J. Chase, P. Docherty, J. Revie, T. Desaive, Structural identifiability analysis of a cardiovascular system model, Med. Eng. Phys. 38 (2016) 433–441.
[27] L. Ellwein, H. Tran, C. Zapata, V. Novak, M. Olufsen, Sensitivity analysis and model assessment: mathematical models for arterial blood flow and blood pressure, Cardiovasc. Eng. 8 (2008) 94–108.
[28] R. Gul, Mathematical modeling and sensitivity analysis of lumped-parameter model of the human cardiovascular system, The Free University, Berlin, Germany, 2016 , Ph.D. Thesis.
[29] V. Eck, W. Donders, J. Sturdy, J. Feinberg, T. Delhaas, L. Hellevik, W. Huberts, A guide to uncertainty quantification and sensitivity analysis for cardiovascular applications, Num. Meth. Biomed. Eng. (2016), https://doi.org/10.1002/cnm.2755.
[30] P. Chen, A. Quarteroni, G. Rozza, Simulation-based uncertainty quantification of human arterial network hemodynamics, Int. J. Numer. Meth. Biomed. Eng. 29 (2013) 698–721.
[31] A. Arnold, C. Battista, D. Bia, Y. Zocalo, R. Armentano, H. Tran, M. Olufsen, Uncertainty quantification in a patient-specific one-dimensional arterial network model: ENKF-based inflow estimator, J. Verif. Valid. Uncert 2 (1) (2017) 011002.
[32] V. Eck, J. Feinberg, H. Langtangen, L. Hellevik, Stochastic sensitivity analysis for timing and amplitude of pressure waves in the arterial system, Int. J. Numer. Meth. Biomed. Eng. (2015), https://doi.org/10.1002/cnm.2711.
[33] V. Eck, J. Feinberg, H. Langtangen, L. Hellevik, Stochastic sensitivity analysis for timing and amplitude of pressure waves in the arterial system, Int. J. Num. Meth. Biomed. Eng. 31 (2015) e02711.
[34] V.G. Eck, W.P. Donders, J. Sturdy, J. Feinberg, T. Delhaas, L.R. Hellevik, W. Huberts, A guide to uncertainty quantification and sensitivity analysis for cardiovascular applications, Int J Num Meth Biomed Eng 32 (2016) e02755.
[35] M. Paun, M.U. Qureshi, M. Colebank, N. Hill, D. Husmeier, MCMC Methods for inference in a mathematical model of pulmonary circulation, Statistica Neerlandica, (2018). Accepted for publication.
[36] H. Haario, M. Laine, A. Mira, E. Saksman, Dram: efficient adaptive MCMC, Stat. Comput. 16 (2006) 339–354.
[37] W. Heimisch, H. Schad, R. Günzinger, Left ventricular volume measurement by the conductance catheter and variations in the hematocrit in small animals, Cardiovasc. Eng. 7 (2) (2007) 43–46.
[38] J. Kjaergaard, C.L. Petersen, A. Kjaer, B.K. Schaadt, J.K. Oh, C. Hassager, Evaluation of right ventricular volume and function by 2d and 3d echocardiography compared to MRI, Eur. J. Echocardiogr. 7 (2006) 430–438.
[39] H.S. Hwang, M.O. Boluyt, K. Converso, M.W. Russell, B.E. Bleske, Effects of hawthorn on the progression of heart failure in a rat model of aortic constriction, Pharmacotherapy 29 (2009) 639–648.
[40] B. Cosyns, S. Droogmans, C. Weytjens, T. Lahoutte, G. Van Camp, D. Schoors, P.R. Franken, Effect of streptozotocin-induced diabetes on left ventricular function in adult rats: an in vivo pinhole gated spect study, Cardiovasc. Diabetol. 6 (2007) 30.
[41] A.I. Al-Shafei, R.G. Wise, G. Gresham, T. Carpenter, L. Hall, C.L.-H. Huang, Magnetic resonance imaging analysis of cardiac cycle events in diabetic rats: the effect of angiotensin-converting enzyme inhibition, J. Physiol. 538 (2002) 555–572.
[42] J. Holt, E. Rhode, H. Kines, Ventricular volumes and body weight in mammals, Am. J. Physiol. 215 (1968) 704–715.
[43] P. Nordbeck, L. Bönhof, K.-H. Hiller, S. Voll, P. Arias-Loza, L. Seidlmayer, T. Williams, Y.-X. Ye, D. Gensler, T. Pelzer, et al., Impact of thoracic surgery on cardiac morphology and function in small animal models of heart disease: a cardiac MRI study in rats, PLoS ONE 8 (2013) e68275.
[44] S.E. Litwin, T.E. Raya, P.G. Anderson, C.M. Litwin, R. Bressler, S. Goldman, Induction of myocardial hypertrophy after coronary ligation in rats decreases ventricular dilatation and improves systolic function. Circulation 84 (1991) 1819–1827.
[45] S.K. Engle, P.F. Solter, K.M. Credille, C.M. Bull, S. Adams, M.J. Berna, A.E. Schultze, E.C. Rothstein, M.D. Cockman, M.L. Pritt, et al., Detection of left ventricular hypertrophy in rats administered a peroxisome proliferator–activated receptor α/γ dual agonist using natriuretic peptides and imaging, Toxicol. Sci. 114 (2009) 183–192.
[46] R. Wise, C.-H. Huang, G. Gresham, A. Al-Shafei, T. Carpenter, L. Hall, Magnetic resonance imaging analysis of left ventricular function in normal and spontaneously hypertensive rats, J. Physiol. 513 (1998) 873–887.
[47] M. Nahrendorf, F. Wiesmann, K.-H. Hiller, K. Hu, C. Waller, J. Ruff, T.E. Lanz, S. Neubauer, A. Haase, G. Ertl, et al., Serial cine-magnetic resonance imaging of left ventricular remodeling after myocardial infarction in rats, J. Magn. Res. Imaging 14 (2001) 547–555.
[48] C. Vanhove, T. Lahoutte, M. Defrise, A. Bossuyt, P.R. Franken, Reproducibility of left ventricular volume and ejection fraction measurements in rat using pinhole gated spect, Eur. J. Nucl. Med. Mol. Imaging 32 (2005) 211–220.
[49] M.P. Bal, W. Vries, F. Leij, M. Oosterhout, J. Baan, E. Wall, F. Bel, P. Steendijk, Left ventricular pressure–volume relationships during normal growth and development in the adult rat–studies in 8-and 50-week-old male wistar rats, Acta Physiol. 185 (2005) 181–191.
[50] M. Nahrendorf, K.-H. Hiller, A. Greiser, S. Köhler, T. Neuberger, K. Hu, C. Waller, M. Albrecht, S. Neubauer, A. Haase, et al., Chronic coronary artery stenosis induces impaired function of remote myocardium: MRI and spectroscopy study in rat, Am. J. Physiol. 285 (2003) H2712–H2721.
[51] T. Radovits, A. Oláh, Á. Lux, B.T. Németh, L. Hidi, E. Birtalan, D. Kellermayer, C. Mátyás, G. Szabó, B. Merkely, Rat model of exercise-induced cardiac hypertrophy: hemodynamic characterization using left ventricular pressure-volume analysis, Am. J. Physiol. 305 (2013) H124–H134.
[52] S. Korkmaz-Icöz, A. Lehner, S. Li, A. Vater, T. Radovits, M. Brune, M. Ruppert, X. Sun, P. Brlecic, M. Zorn, et al., Left ventricular pressure-volume measurements and myocardial gene expression profile in type-2 diabetic goto-kakizaki rats, Am. J. Physiol. (2016) ajpheart–00956.
[53] A. Todica, G. Böning, S. Lehner, E. Weidl, P. Cumming, C. Wängler, S.G. Nekolla, M. Schwaiger, P. Bartenstein, R. Schirrmacher, et al., Positron emission tomography in the assessment of left ventricular function in healthy rats: a comparison of four imaging methods, J. Nucl. Cardiol. 20 (2013) 262–274.
[54] C.A. Carr, D.J. Stuckey, L. Tatton, D.J. Tyler, S.J. Hale, D. Sweeney, J.E. Schneider, E. Martin-Rendon, G.K. Radda, S.E. Harding, et al., Bone marrow-derived stromal cells home to and remain in the infarcted rat heart but fail to improve function: an in vivo cine-MRI study, Am. J. Physiol. 295 (2008) H533–H542.
[55] J.R. Jones, J.F. Mata, Z. Yang, B.A. French, J.N. Oshinski, Left ventricular remodeling subsequent to reperfused myocardial infarction: evaluation of a rat model using cardiac magnetic resonance imaging, J. Cardiovasc. Magn. Res. 4 (2002) 317–326.
[56] D.J. Stuckey, C.A. Carr, D.J. Tyler, E. Aasum, K. Clarke, Novel MRI method to detect altered left ventricular ejection and filling patterns in rodent models of disease, Magn. Res. Med. 60 (2008) 582–587.
[57] J.-L. Daire, J.-P. Jacob, J.-N. Hyacinthe, P. Croisille, K. Montet-Abou, S. Richter, D. Botsikas, M. Lepetit-Coiffé, D. Morel, J.-P. Vallée, Cine and tagged cardiovascular magnetic resonance imaging in normal rat at 1.5 t: a rest and stress study, J. Cardiovasc. Magn. Res. 10 (2008) 48.
[58] M. Ruppert, S. Korkmaz-Icöz, S. Li, B.T. Németh, P. Hegedűs, P. Brlecic, C. Mátyás, M. Zorn, B. Merkely, M. Karck, et al., Myocardial reverse remodeling after pressure unloading is associated with maintained cardiac mechanoenergetics in a rat model of left ventricular hypertrophy, Am. J. Physiol. 311 (2016) H592–H603.
[59] N. Trippodo, Total circulatory capacity in the rat. Effects of epinephrine and

vasopressin on compliance and unstressed volume. Circ. Res. 49 (1981) 923–931.
[60] D.B. Young, San Rafael (CA): Morgan & Claypool Life Sciences, (2010).
[61] S. Gelman, Venous function and central venous pressurea physiologic story, J. Am. Soc. Anesthesiol. 108 (2008) 735–748.
[62] J.E.W. Beneken, B. DeWit, A physical approach to hemodynamic aspects of the human cardiovascular system, Physical Bases of Circulatory Transport, W.B. Saunders, Philadelphia, Pa, USA, 1967, pp. 1–45.
[63] R.J. Gotwals, Cardiovascular Physiology: The Windkessel Model, (2003), https://shodor.org/succeed-1.0/biomed/labs/windk.html.
[64] R.E. Klabunde, Cardiovascular Physiology Concepts, Wolters Kluwer, Lippincott, Williams & Wilkins, Philadelphia, USA, 2014.
[65] G. London, A.C. Simon, Y. Weiss, M.E. Safar, Arterial and Venous systems in Essential Hypertension, 63 Springer Science & Business Media, 2012.
[66] I.C. Ipsen, C. Kelley, S. Pope, Rank-deficient nonlinear least squares problems and subset selection, SIAM J. Numer. Anal. 49 (2011) 1244–1266.
[67] H. Miao, X. Xia, A. Perelson, H. Wu, On identifiability of nonlinear ode models and applications in viral dynamics, SIAM Rev. 53 (2011) 3–39.
[68] J.T. Ottesen, J. Mehlsen, M.S. Olufsen, Structural correlation method for model reduction and practical estimation of patient specific parameters illustrated on heart rate regulation, Math. Biosci. 257 (2014) 50–59.
[69] C.T. Kelley, Iterative Methods for Optimization, 18 SIAM, 1999.
[70] R.C. Smith, Uncertainty Quantification: Theory, Implementation, and Applications, 12 SIAM, 2013.
[71] S. Smolyak, Quadrature and interpolation formulas for tensor products of certain classes of functions, Sov. Phys. Dokl. 148 (1963) 1042–1045.
[72] H.-J. Bungartz, M. Griebel, Sparse grids, Acta Numerica 13 (2004) 147–269.
[73] J. Halton, On the efficiency of certain quasi-random sequences of points in evaluating multi-dimensional integrals, Numerische Mathematik 2 (1960) 84–90.
[74] S. Joe, F. Kuo, Remark on algorithm 659: implementing sobol's quasirandom sequence generator, ACM Trans. Math. Softw. (TOMS) 29 (2003) 49–57.
[75] C. Andrieu, J. Thoms, A tutorial on adaptive MCMC, Stat. Comput. 18 (2008) 343–373.
[76] A. Mira, On metropolis-hastings algorithm with delayed rejection, Metron LIX (2001) 231–241.
[77] H. Haario, E. Saksman, J. Tamminen, An adaptive metropolis algorithm, Bernoulli 7 (2001) 223–242.
[78] J. Ottesen, M. Olufsen, A practical approach to parameter estimation applied to model predicting heart rate regulation, J. Math. Biol. 67 (2013) 39–68.
[79] B. Smith, J. Chase, R. Nokes, G. Shaw, G. Wake, Minimal haemodynamic system model including ventricular interaction and valve dynamics, Med. Eng. Phys. 26 (2004) 131–139.
[80] K. Lu, J. Clark, F. Ghorbel, D. Ware, A. Bidani, A human cardiopulmonary system model applied to the analysis of the valsalva maneuver, Am. J. Physiol. 281 (2001) H26612679.
[81] C. Puelz, S. Acosta, B. Riviere, D. Penny, B. KM, C. Rusin, A computational study of the Fontan circulation with fenestration or hepatic vein exclusion, Comput. Biol. Med. 89 (2017) 405–418.
[82] A. Guyton, T. Coleman, H. Granger, Circulation: overall regulation, Annu. Rev. Physiol. 34 (1972) 13–46.
[83] R. Spiegel, Stressed vs. unstressed volume and its relevance to critical care practitioners, Clin. Exp. Emerg. Med. 3 (2016) 52–54.
[84] Y. Sun, B. Sjoberg, P. Ask, D. Loyd, B. Wranne, Mathematical model that characterizes transmitral and pulmonary venous flow velocity patterns, Am. J. Physiol. Heart Circ. Physiol. 268 (1995) H476–H489.
[85] B.W. Smith, J.G. Chase, R.I. Nokes, G.M. Shaw, G. Wake, Minimal haemodynamic system model including ventricular interaction and valve dynamics, Med. Eng. Phy. 26 (2004) 131–139.
[86] J. Mynard, M. Davidson, D. Penny, J. Smolich, A simple, versatile valve model for use in lumped parameter and one-dimensional cardiovascular models, Int. J. Numer. Meth. Biomed. Eng. 28 (2012) 626–641.
[87] R.J. LeVeque, Finite Difference Methods for Ordinary and Partial Differential Equations: Steady-State and Time-Dependent Problems, SIAM, 2007.
[88] A. Iserles, A First Course in the Numerical Analysis of Differential Equations, Cambridge University Press, 2008.
[89] C. Olsen, Modeling heart rate regulation by the baroreflex, NC State University, Raleigh, NC, 2014 , Ph.D. thesis.
[90] J.R. Martins, P. Sturdza, J.J. Alonso, The complex-step derivative approximation, ACM Trans. Math. Softw. (TOMS) 29 (2003) 245–262.
[91] H. Banks, S. Dediu, S. Ernstberger, F. Kappel, Generalized sensitivities and optimal experimental design, J. Inv. Ill-posed Probl. 18 (2010) 25–83.
[92] R. Hovorka, P. Vicini, Parameter estimation, Mod. Meth. Phys. Med. (2001) 107–151.
[93] D. Schiavazzi, G. Arbia, C. Baker, A.M. Hlavacek, T.-Y. Hsia, A. Marsden, I. Vignon-Clementel, et al., Uncertainty quantification in virtual surgery hemodynamics predictions for single ventricle palliation, Int. J. Numer. Method Biomed. Eng. 32 (2016).
[94] P. Chen, A. Quarteroni, G. Rozza, Simulation-based uncertainty quantification of human arterial network hemodynamics, Int. J. Numer. Method Biomed. Eng. 29 (2013) 698–721.
[95] S. Sankaran, H.J. Kim, G. Choi, C.A. Taylor, Uncertainty quantification in coronary blood flow simulations: impact of geometry, boundary conditions and blood viscosity, J. Biomech. 49 (2016) 2540–2547.
[96] P. Pathmanathan, M.S. Shotwell, D.J. Gavaghan, J.M. Cordeiro, R.A. Gray, Uncertainty quantification of fast sodium current steady-state inactivation for multi-scale models of cardiac electrophysiology, Prog. Biophys. Mol. Biol. 117 (2015) 4–18.
[97] J.P. Kaipio, E. Somersalo, Statistical and Computational Inverse Problems, Springer, New York, 2005.
[98] J. Liu, M. West, Combined parameter and state estimation in simulation-based filtering, in: A. Doucet, N. de Freitas, N. Gordon (Eds.), Sequential Monte Carlo Methods in Practice, Springer, New York, 2001, pp. 197–223.
[99] M. Pitt, N. Shephard, Filtering via simulation: auxiliary particle filters, J. Am. Stat. Assoc. 94 (1999) 590–599.
[100] A. Arnold, D. Calvetti, E. Somersalo, Linear multistep methods, particle filtering and sequential monte carlo, Inv. Probl. 29 (2013) 085007.
[101] G. Evensen, Sequential data assimilation with a nonlinear quasi-geostrophic model using monte carlo methods to forecast error statistics, J. Geophys. Res. 99 (1994) 10143–10162.
[102] G. Burgers, P.J. Leeuwen, G. Evensen, Analysis scheme in the ensemble kalman filter, Mon. Weather Rev. 126 (1998) 1719–1724.
[103] G. Evensen, The ensemble Kalman filter for combined state and parameter estimation, IEEE Control Syst. Mag. 29 (2009) 83–104.
[104] A. Arnold, D. Calvetti, E. Somersalo, Parameter estimation for stiff deterministic dynamical systems via ensemble Kalman filter, Inv. Probl. 30 (2014) 105008.
[105] C.E. Rasmussen, C.K. Williams, Gaussian processes for machine learning, 1 MIT Press Cambridge, 2006.
[106] M.K. Cowles, B.P. Carlin, Markov chain monte carlo convergence diagnostics: a comparative review, J. Am. Stat. Assoc. 91 (1996) 883–904.